The chronology of mysticete diversification (Mammalia, Cetacea, Mysticeti): Body size, morphological evolution and global change

The chronology of mysticete diversification (Mammalia, Cetacea, Mysticeti): body size, morphological evolution and global change

Bisconti M.[1,2,*], Pellegrino L.[1], Carnevale G.[1]

[1]Dipartimento di Scienze della Terra, Università degli Studi di Torino, via Valperga Caluso 35, 10100, Torino, Italy

[2]San Diego Natural History Museum, 1788 El Prado, San Diego, 92292 California, USA

[*]Corresponding author: Michelangelo Bisconti, e-mail: michelangelo.bisconti@unito.it

RUNNING TITLE: Chronology and evolution of mysticete clades

Abstract

A comprehensive revision of the localities of discovery of fossil mysticetes is presented together with a highly inclusive phylogenetic analysis in order to provide the basis for a chronology of the main mysticete diversification events. The results suggest that the origin of Mysticeti (that include earlier toothed taxa together with today baleen-bearing cetaceans) occurred *c.* 38 Ma; the origin of Chaeomysticeti (that include only baleen-bearing cetaceans) occurred *c.* 28 Ma; the origin of Balaenomorpha (crown mysticetes) occurred *c.* 23.3 Ma. Additional chronological inferences are provided. Within this chronological framework, we analyzed diversity trends, origination and extinction patterns and body size evolution, and looked for eventual causal relationships between evolutionary processes, marine and terrestrial ecological turnovers and geodynamic events. We found five main diversification events corresponding to peaks in originations and, in a few cases, with the origin of different feeding strategies adopted by the differen mysticete families. We found that different mechanisms are correlated to specific diversification events and these include changes in temperature and ocean circulation patterns, nutrient availability in the water column and diatom abundance and diversity. Resuming, no single mechanism explains all the diversification events occurred during mysticete evolution; rather, we found that each diversification event was correlated to different combinations of biotic and abiotic factors, suggesting that this group experienced major adaptation process to the changing paleoenvironments in the last 38 Ma.

Figure

Click here to access/download;Figure;Fig. 1 R1.jpg

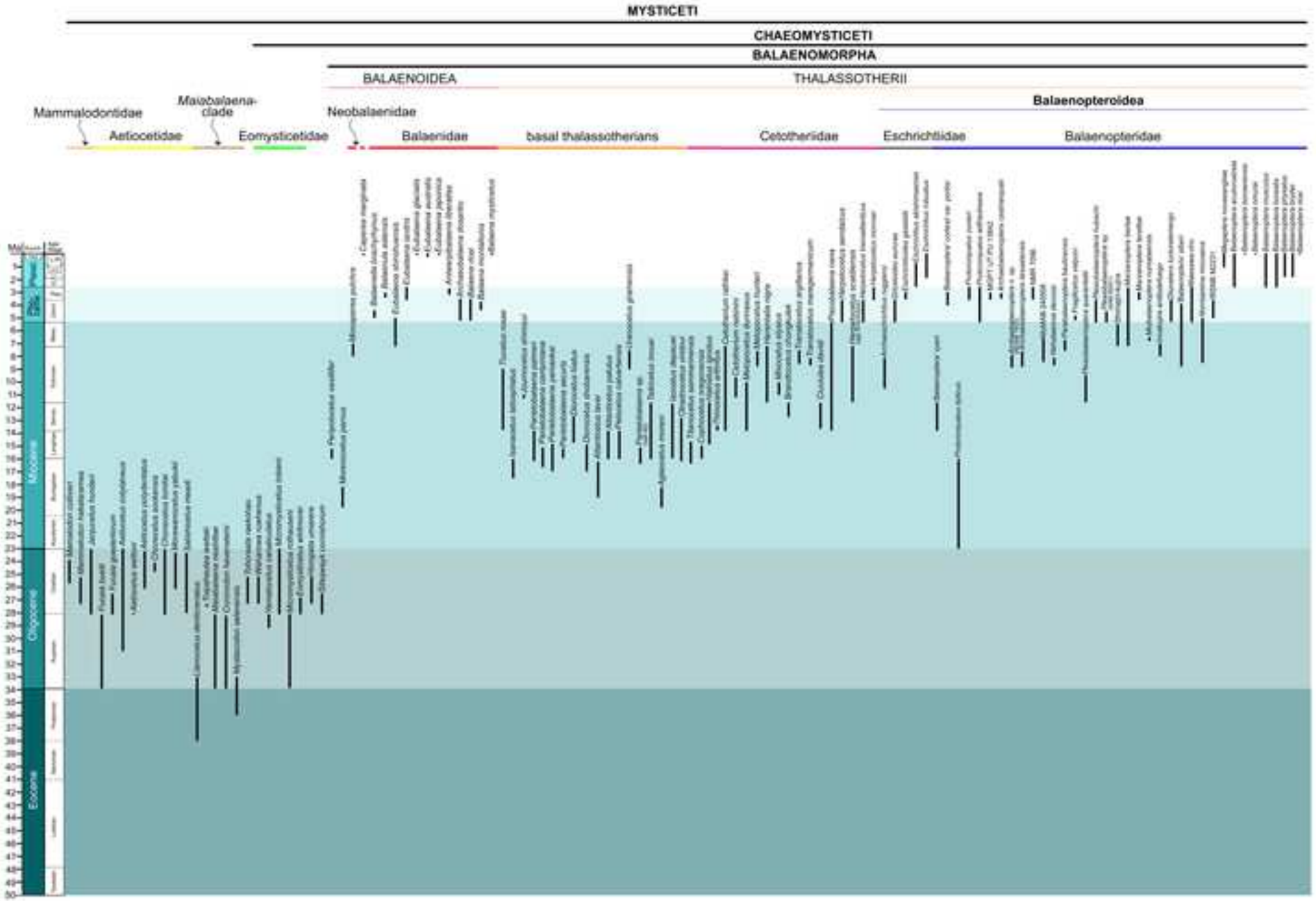

Figure

Click here to access/download;Figure;Fig. 2 R1.jpg

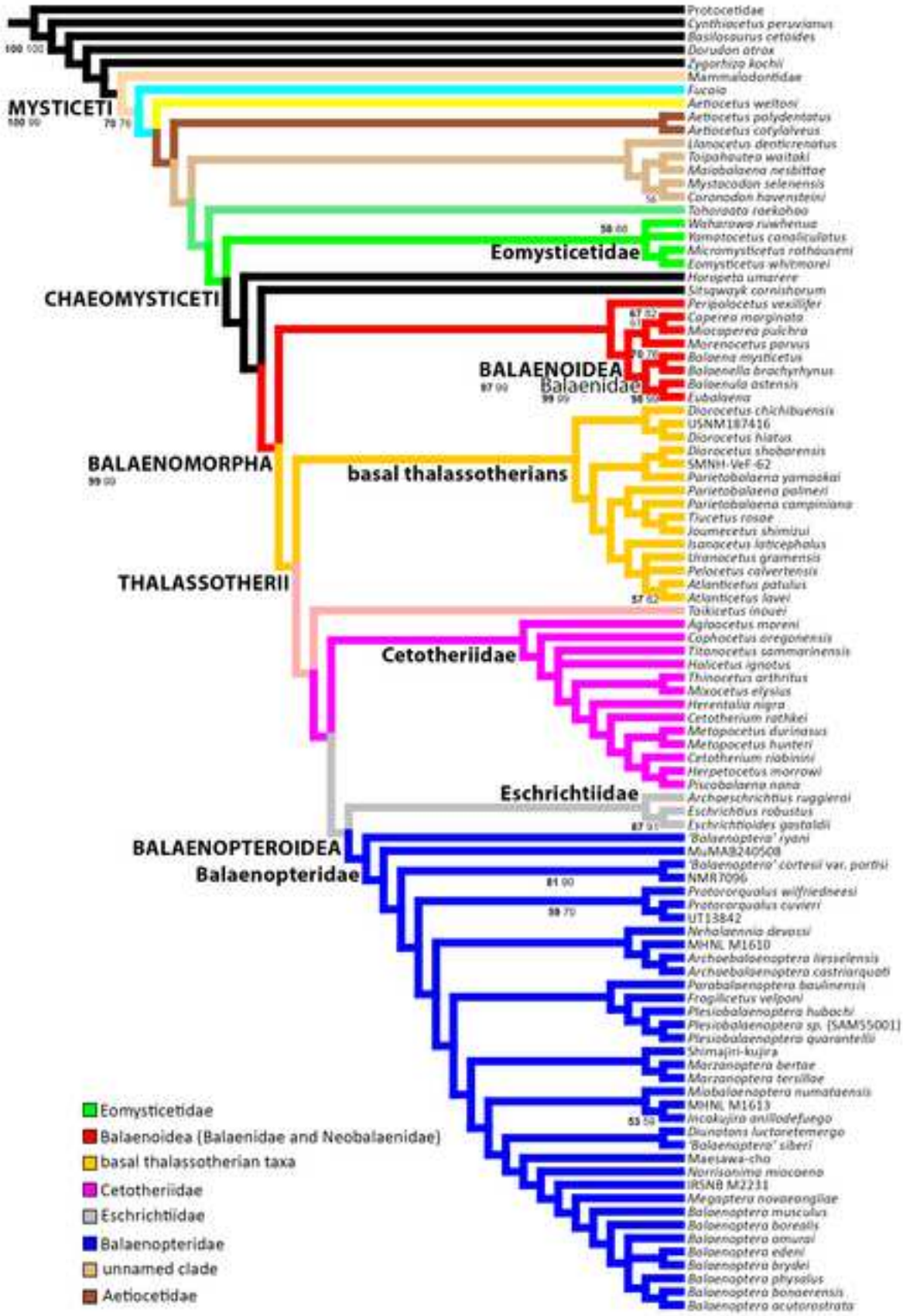

Figure

Click here to access/download;Figure;Fig. 3.jpg

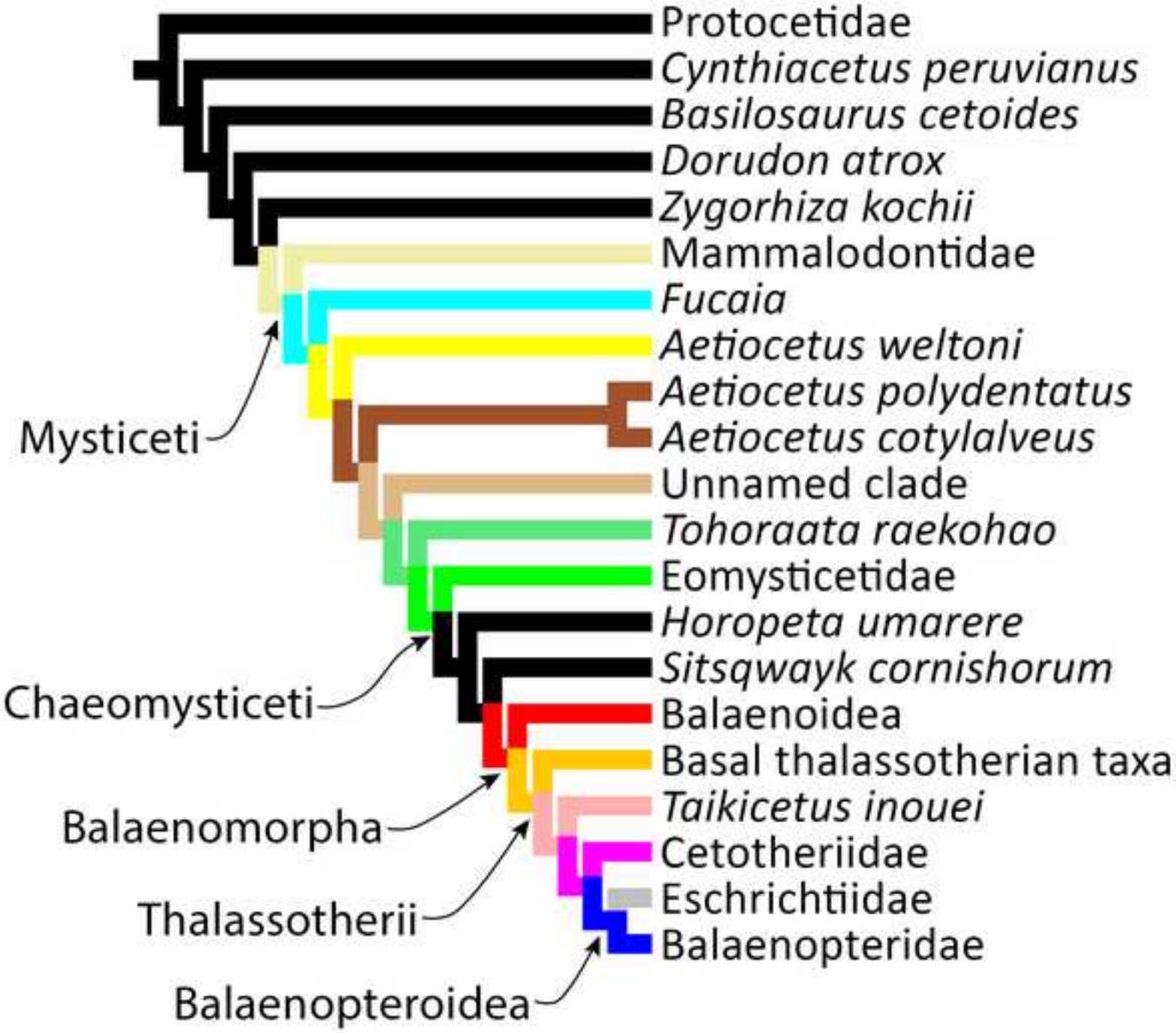

Figure

Click here to access/download;Figure;Fig. 4 R1.jpg

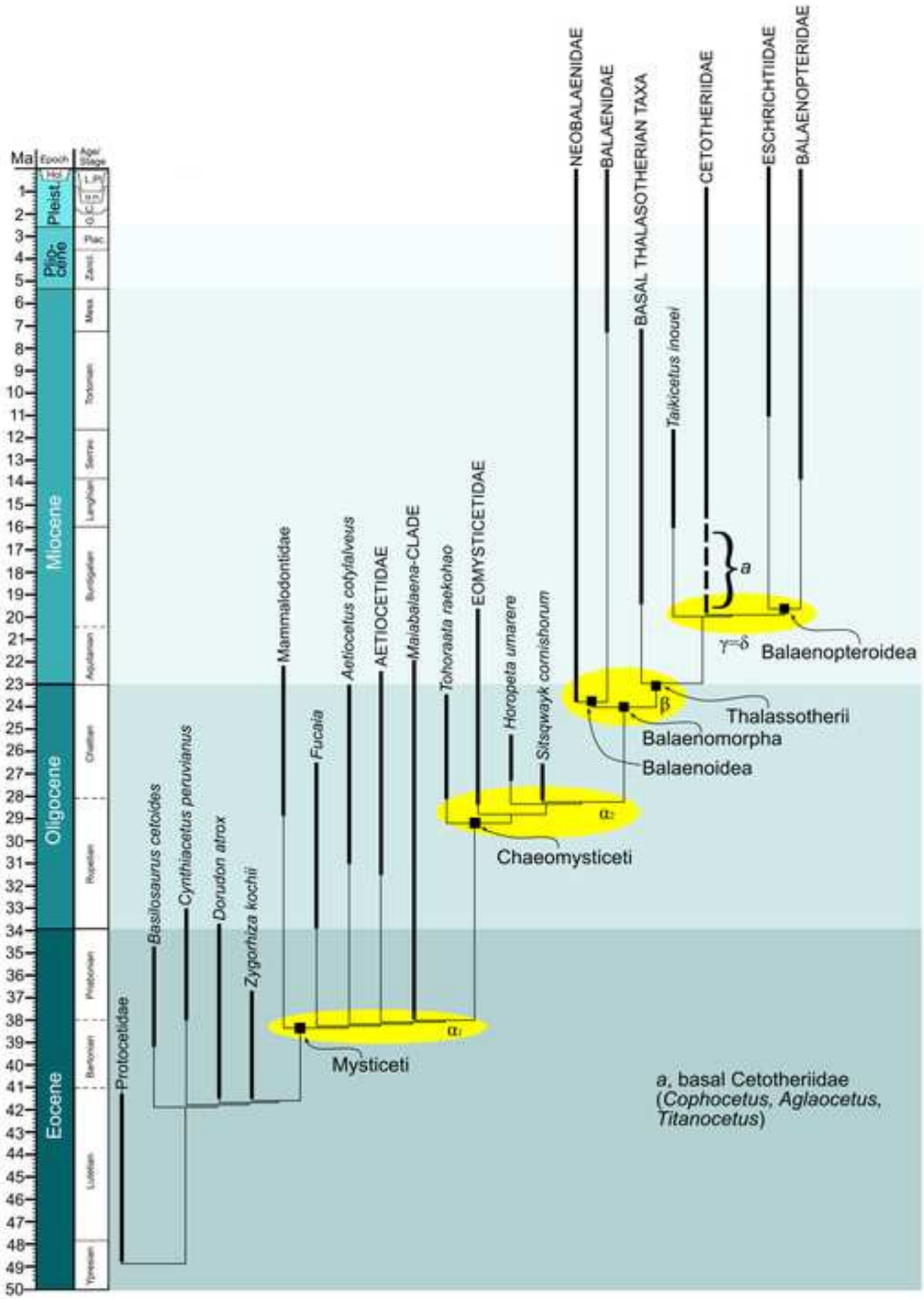

Figure

Click here to access/download;Figure;Fig. 5 R1.jpg

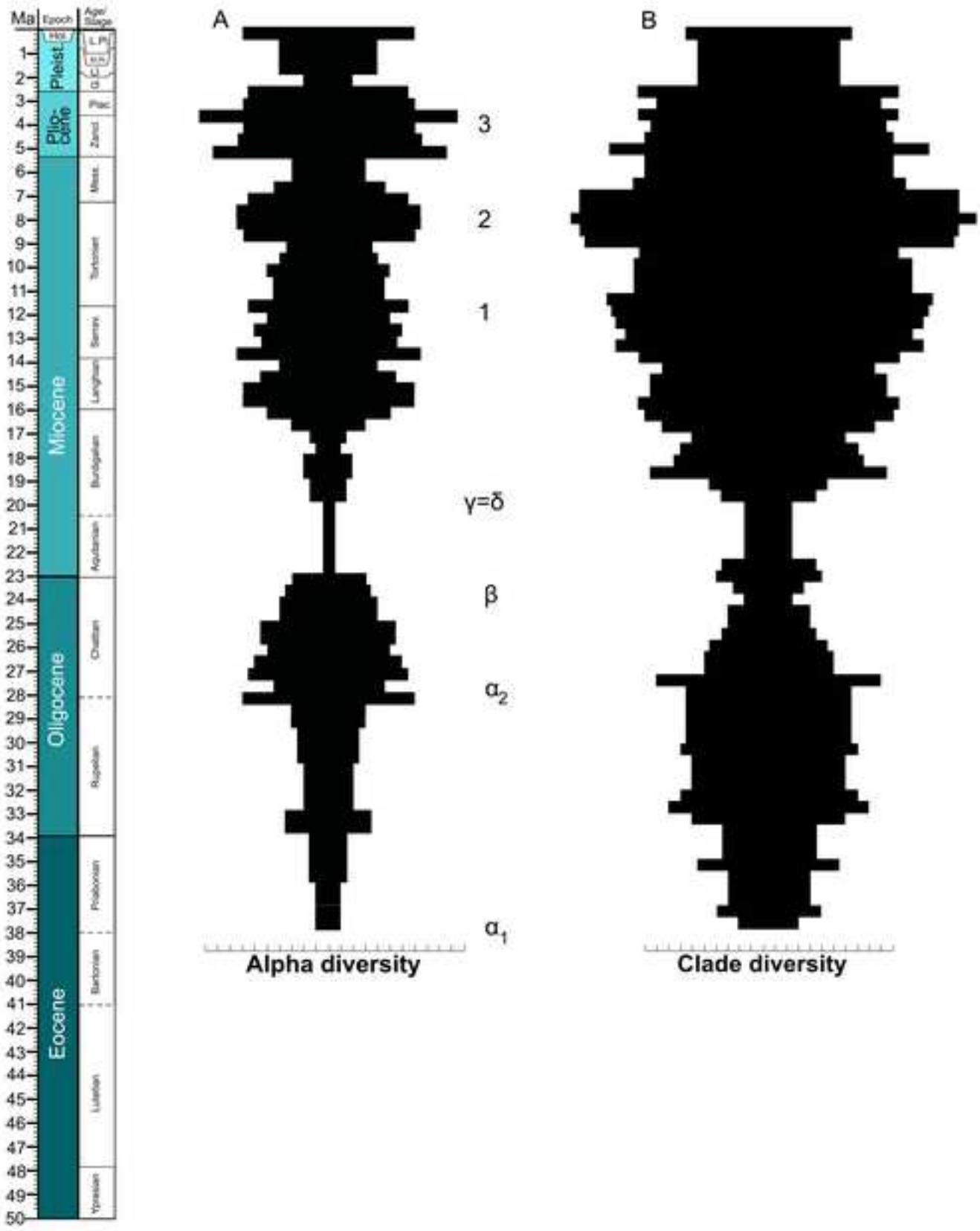

Figure

Click here to access/download;Figure;Fig. 6 R1 j.jpg

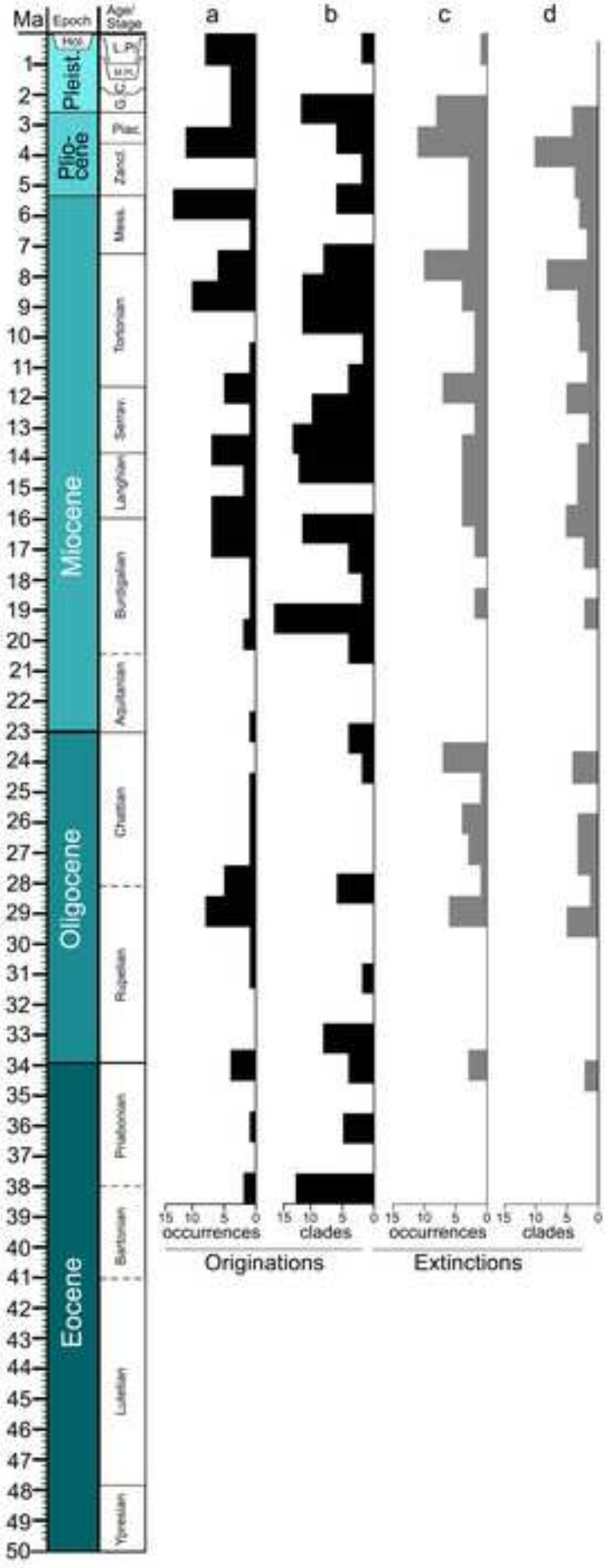

Figure

Click here to access/download;Figure;Fig. 7.jpg

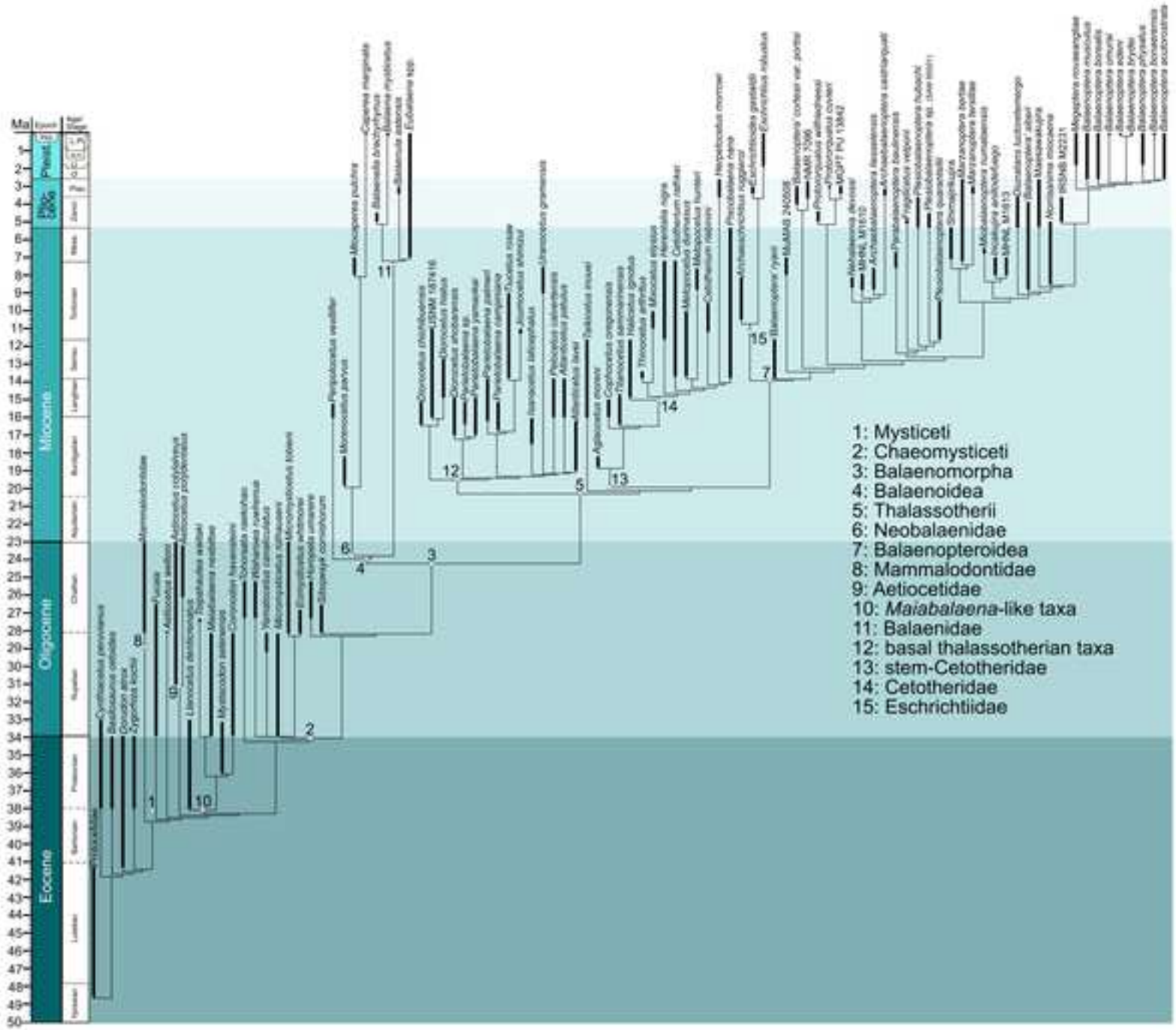

Figure

Click here to access/download;Figure;Fig. 8 R1.jpg

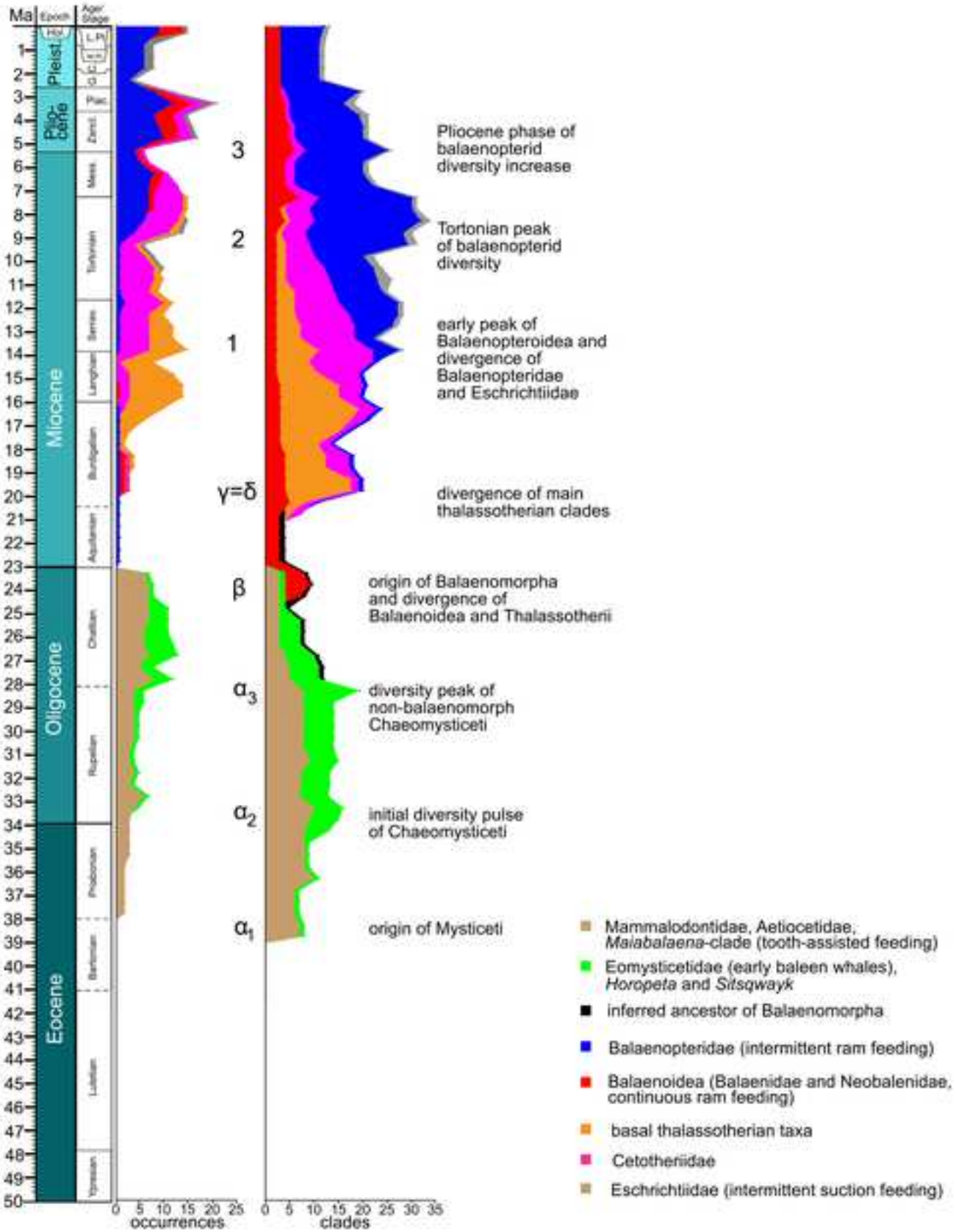

Figure

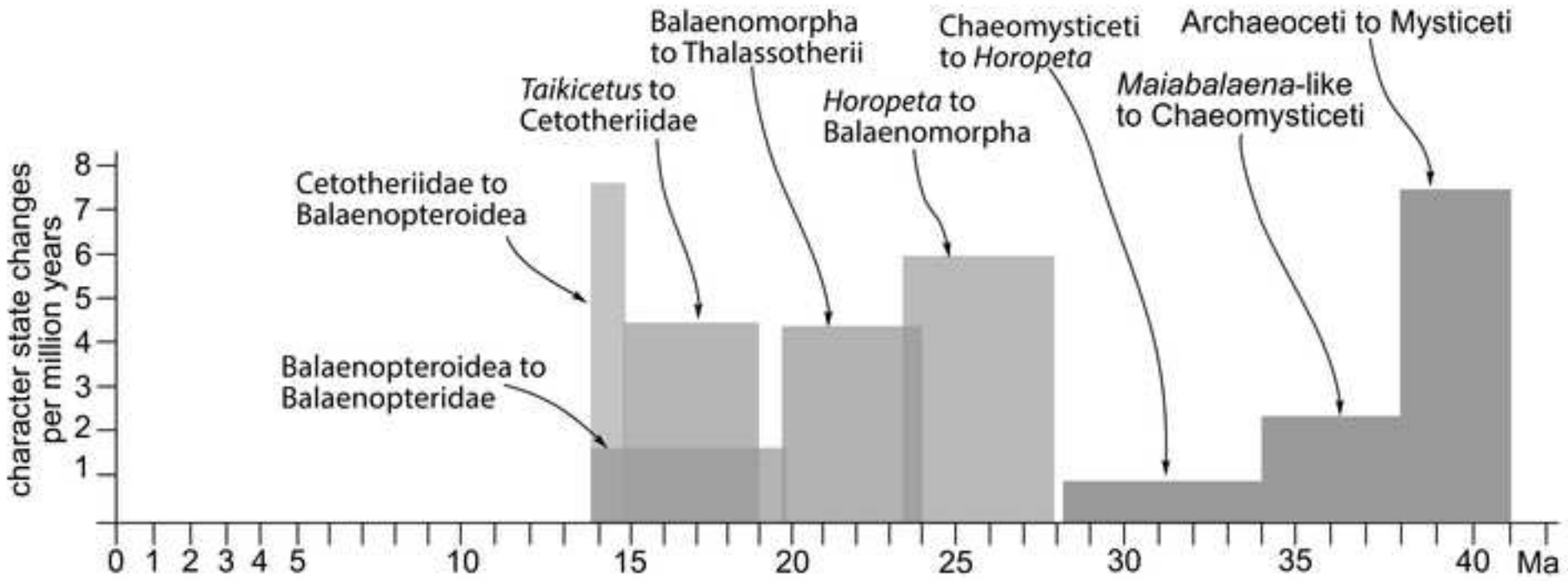

Figure

Click here to access/download;Figure;Fig. 10 R1.jpg

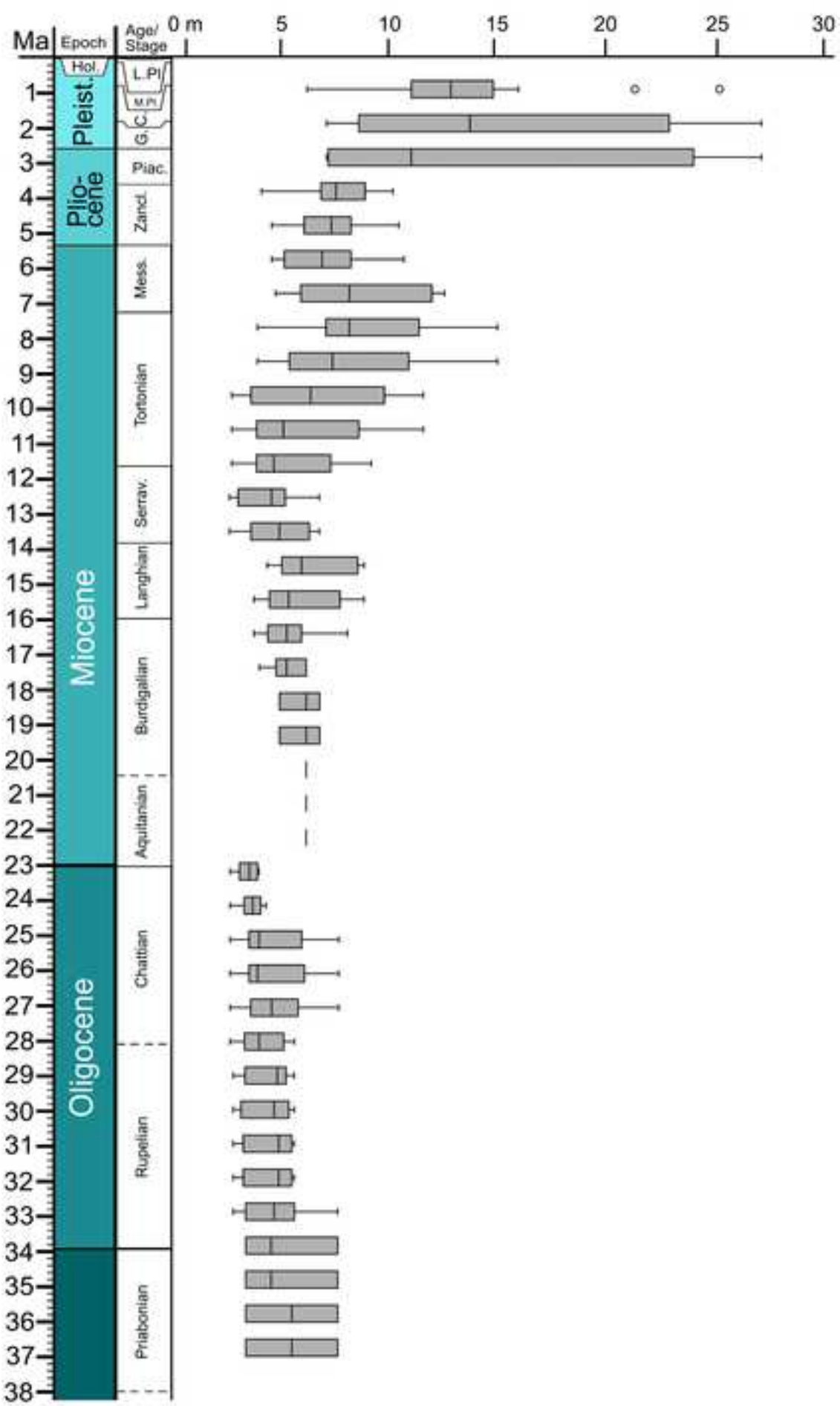

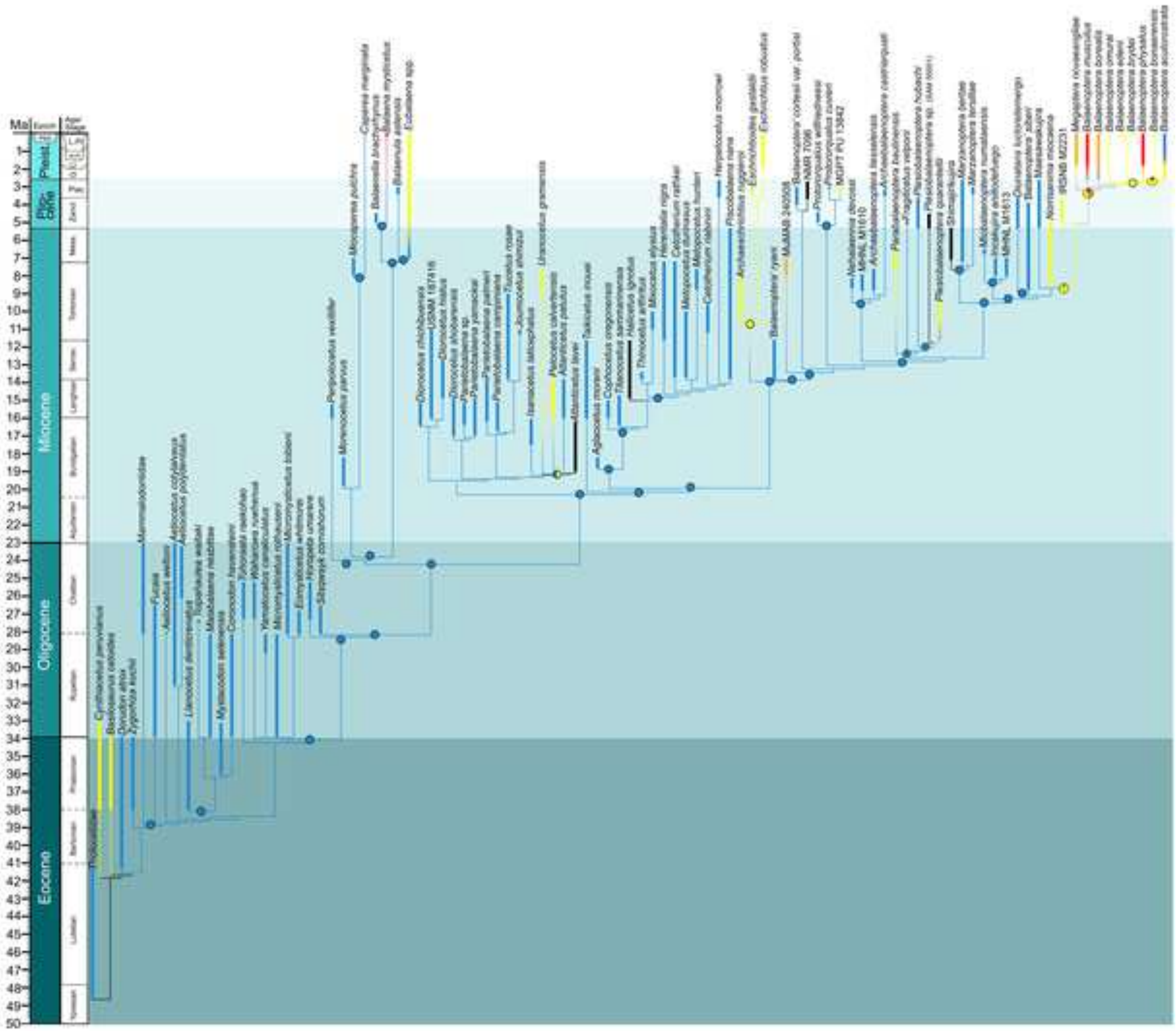

Figure

Click here to access/download;Figure;Fig. 12.jpg

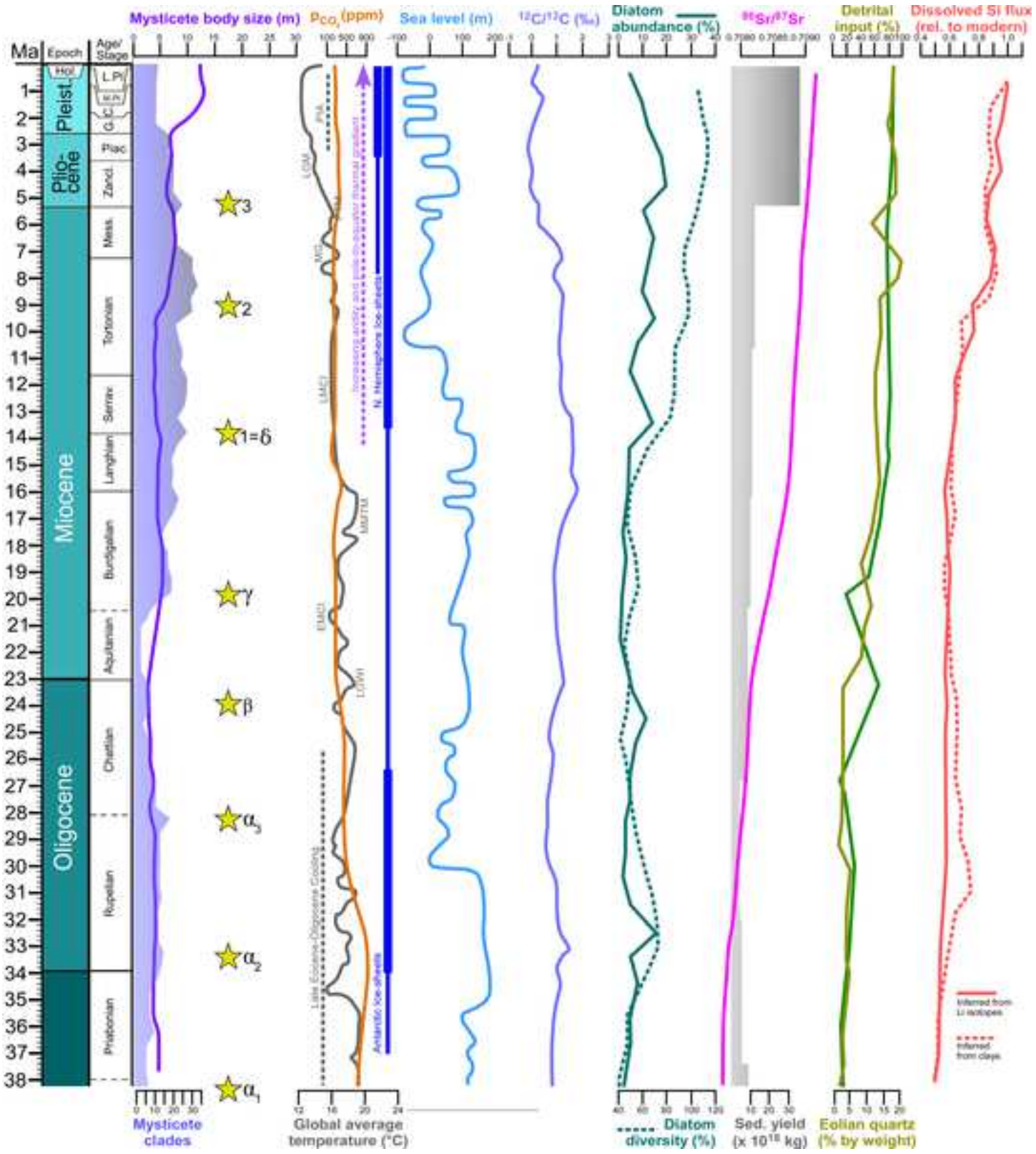

Figure

Click here to access/download;Figure;Fig. 13.jpg

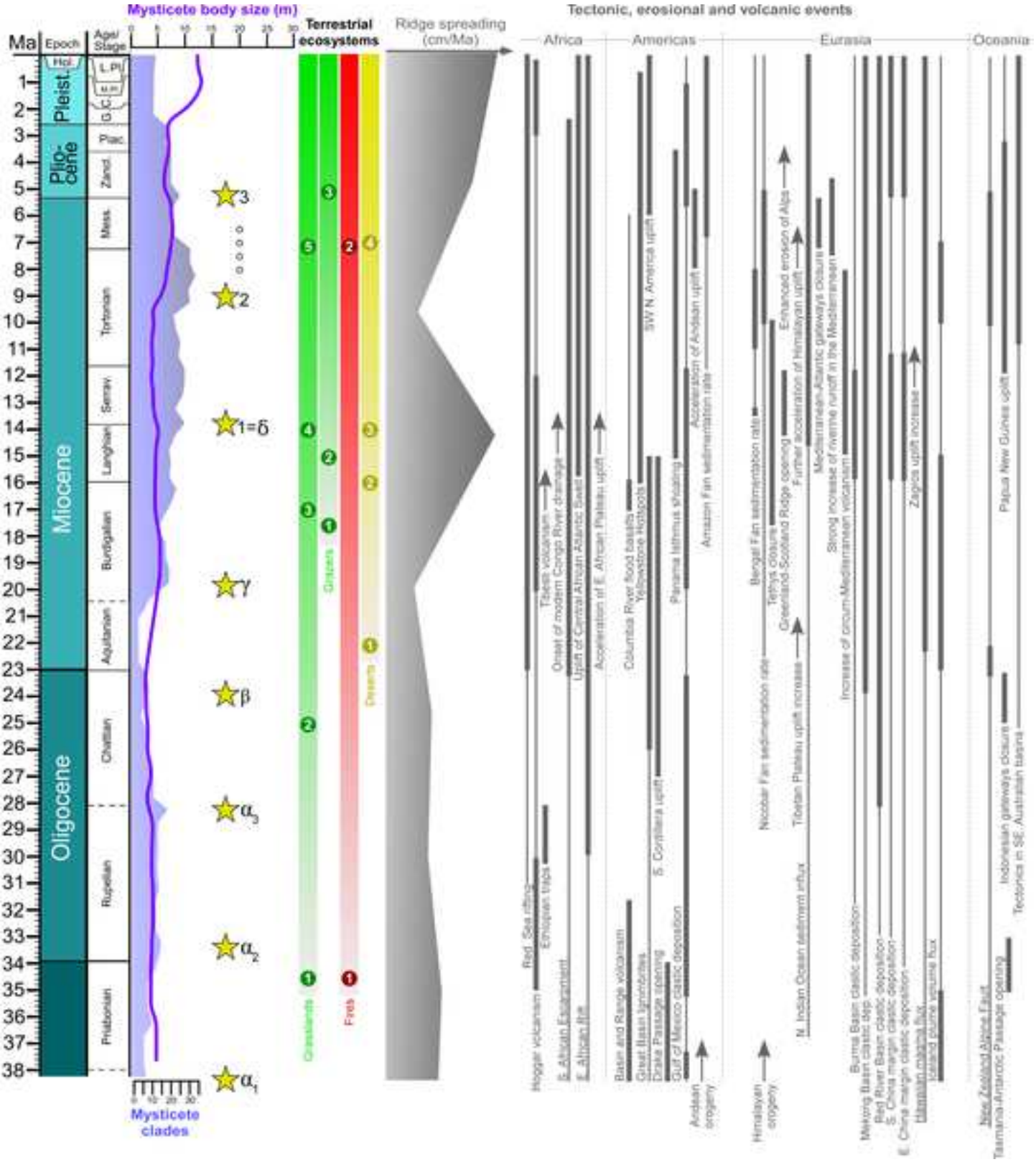

Figure

Click here to access/download;Figure;Fig. 14.jpg

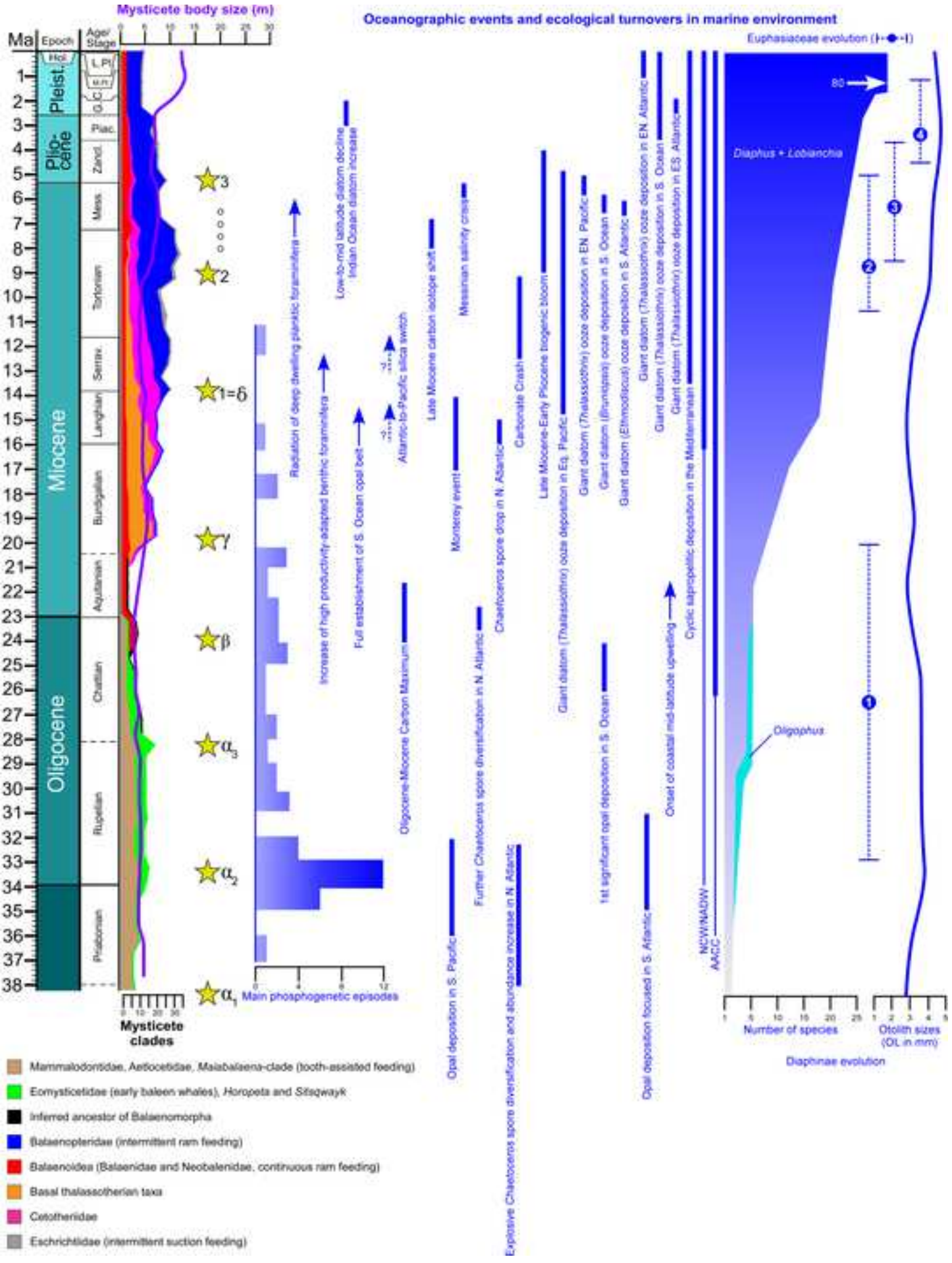

Declaration of interests

☒The authors declare that they have no known competing financial interests or personal relationships that could have appeared to influence the work reported in this paper.

☐The authors declare the following financial interests/personal relationships which may be considered as potential competing interests:

The chronology of mysticete diversification (Mammalia, Cetacea, Mysticeti): body size, morphological evolution and global change

Bisconti M.[1,2,*], Pellegrino L.[1], Carnevale G.[1]

[1]Dipartimento di Scienze della Terra, Università degli Studi di Torino, via Valperga Caluso 35, 10100, Torino, Italy

[2]San Diego Natural History Museum, 1788 El Prado, San Diego, 92292 California, USA

[*]Corresponding author: Michelangelo Bisconti, e-mail: michelangelo.bisconti@unito.it

RUNNING TITLE: Chronology and evolution of mysticete clades

Abstract

A comprehensive revision of the localities of discovery of fossil mysticetes is presented together with a highly inclusive phylogenetic analysis in order to provide the basis for a chronology of the main mysticete diversification events. The results suggest that the origin of Mysticeti (that include earlier toothed taxa together with today baleen-bearing cetaceans) occurred *c.* 38 Ma; the origin of Chaeomysticeti (that include only baleen-bearing cetaceans) occurred *c.* 28 Ma; the origin of Balaenomorpha (crown mysticetes) occurred *c.* 23.3 Ma. Additional chronological inferences are provided. Within this chronological framework, we analyzed diversity trends, origination and extinction patterns and body size evolution, and looked for eventual causal relationships between evolutionary processes, marine and terrestrial ecological turnovers and geodynamic events. We found five main diversification events corresponding to peaks in originations and, in a few cases, with the origin of different feeding strategies adopted by the differen mysticete families. We found that different mechanisms are correlated to specific diversification events and these include changes in temperature and ocean circulation patterns, nutrient availability in the water column and diatom abundance and diversity. Resuming, no single mechanism explains all the diversification events occurred during mysticete evolution; rather, we found that each diversification event was correlated to different combinations of biotic and abiotic factors, suggesting that this group experienced major adaptation process to the changing paleoenvironments in the last 38 Ma.

Key words

Baleen whales, Body size, Chronology, Diversity, Extinction/origination rates, Global change, Phylogeny, Trophic web evolution

1. Introduction

Extant mysticete cetaceans (i.e., baleen-bearing whales) are represented by a handful of species in six genera (Bannister, 2009) but their role in oceanic ecology is of paramount importance. Several lines of evidence showed that mysticetes sequester enormous quantities of Carbon through their ability to perform mass predation on schooling shrimps and fish (Pershing and Stamietzkin, 2020); moreover, they fertilize the oceans by releasing iron and other nutrients contained in their feces so that mysticetes are able to indirectly control the abundance of their prey and the algal component of the oceanic trophic webs (Savoca et al., 2021).

The study of the fossil record revealed that the past mysticete diversity reached levels unrivalled in present time (Berta and Lanzetti, 2020; Bisconti et al., 2019; Marx and Uhen, 2010) suggesting that structural aspects of the oceanic ecosystems of the last million years should have been profoundly different from today. Genetic analyses revealed that the exceptionally high numbers of individuals were in existence slightly before the beginning of the industrial whaling (e.g., Roman and Palumbi, 2003; Rooney et al., 2001) in at least four species (*Balaena mysticetus*, *Balaenoptera acutorostrata*, *B. physalus* and *Megaptera novaeangliae*). This supports the view that we are living at a time of widespread ecological change due, at least partially, to a massive reduction in baleen whale abundance (e.g., Pershing et al., 2010). Understanding the past ecological settings when mysticetes were more abundant represents a good starting point to better understand both the evolutionary history of baleen whales and historical changes in ocean ecology.

Previous studies focused on past mysticete diversity and its relation to diatom abundance, temperature variability, major tectonic events, and nutrient availability in the oceans throughout the Cenozoic (e.g., Bisconti et al. 2021, 2019, 2010; Marx and Fordyce, 2015; Steeman et al., 2009; Marx and Uhen, 2010; Fordyce, 1980, 1977). The analyses led to hypotheses about the eventual existence of causal relationships between diversity and body size change in mysticetes and some paleoclimatic and paleoecological parameters, such as the temperature decline in the Pleistocene and the availability of nutrients supporting biogenic blooms in specific age intervals (Bisconti et al.,

2021; Slater et al., 2017; Marx and Uhen, 2010). Despite these efforts, several questions remain unanswered. It is still unclear the extent of the causal relationships between abiotic and biotic factors in promoting or depressing the diversity of mysticetes in the past as it is not fully understood the role that the fertilizing actions of the mysticete individuals can have had in the past oceanic ecology. Following the theoretical framework of Berge et al. (2012) and the experimental works of Savoca et al. (2021), mysticetes should not be viewed only as passive actors in the oceanic ecosystems but, rather, as active agents of ecosystem engineering able to shape the energy flow between the different parts of the trophic web.

To improve our understanding of the role of baleen whales within their ecosystems, a detailed analysis of their past diversity is necessary in the framework of a more accurate estimate of the timings of their diversification. The latter is a key point because divergence dates of the main mysticete clades are crucial in the understanding of the rates of morphological evolution, rates of body size change, and origination/extinction patterns (e.g., Katz, 2019; Alroy, 2014). In the last two decades, a number of works focused on the inference of divergence dates for major mysticete clades and all were based on molecular or total evidence analyses (e.g., Árnason et al., 2018; Marx and Fordyce, 2015; Geisler et al., 2011; Steeman et al., 2009; McGowen et al., 2009; Sasaki et al., 2005). In these studies, the fossil record was used for calibration of molecular clocks and the results were highly variable. For example, based on molecular and total evidence analyses, the origin of crown mysticetes was inferred to range between 39 (late Eocene) and 29 (early Oligocene) Ma but newly discovered fossils provided evidence that the earliest mysticetes were existent at least since 33 Ma (Fordyce and Marx, 2018; Muizon et al., 2017) thus excluding a younger age for the origin of crown Mysticeti. Again, this undermines the sensitivity of molecular clocks to updated knowledge of the fossil record.

To overcome the problems related to the molecular clocks, we investigated the possibility to infer divergence dates for main mysticete clades by using a statistical method described by Gingerich and Uhen (1998) and subsequently used by Bajpai and Gingerich (1998) and O'Leary and Uhen (1999)

to infer the divergence date of Cetacea from their terrestrial ancestors. The method uses occurrence data (number of localities) to make statements about presence/absence of a given taxon in a given stratigraphic range within an interval of statistical significance. We outline this method in the Material and methods section and direct the reader to O'Leary and Uhen (1999) for a detailed explanation. As detailed occurrence and locality data are available from the Paleobiology Database, we used this method in order to infer the divergence dates of the main mysticete clades including Mysticeti, Chaeomysticeti (baleen-bearing whales), Balaenomorpha (crown Mysticeti), Balaenoidea (right and pygmy right whales), and Balaenopteroidea (rorquals, humpbacks and grey whales). We then used the new divergence dates to assess several parameters emerging from the mysticete fossil record: (a) origination/extinction patterns, (b) diversity patterns, (c) rates of morphological change, and (d) rates of body size change. In the end, we compared our results with data from diatom abundance and diversity, temperature variability, tectonic events, and nutrient availability in order to obtain an integrated view of the possible drivers that concurred to mysticete diversity and evolution throughout most of the Cenozoic.

The advantage of using this method is that it provides ranges of divergence dates that are fully independent from models of molecular evolution and thus it does not suffer from well-known shortcomings of the molecular clocks (see, e.g., Bromham, 2019; Katz, 2019). The disadvantage consists in that the confidence interval of first and last occurrence data for the taxa may be low because it depends on uncertainties about the beginning and duration of worldwide sedimentary processes (Alroy, 2014). To overcome this problem, a detailed review of the mysticete-bearing localities was performed allowing the compilation of the most accurate dataset.

A new and comprehensive phylogenetic analysis of mysticetes was necessary to enable us to contextualize our chronological results within a phylogenetic framework, including as many taxa as possible from as many worldwide localities as possible. Within such a comprehensive phylogenetic framework, we aim at (1) describing the main evolutionary events (morphological change, extinction/origination patterns, body size change) occurred during mysticete evolution, and (2)

investigating into the possible causal relationships between these events and other biotic and abiotic factors to better understand the evolution of the oceanic ecological webs in the last 40 million years.

2. Materials and methods

2.1. Structure of the dataset

The data used in the present paper are available as supplementary online materials. We provided two files (Supplementary File 1 and 2) including what follows. In the Supplementary File 1, we provide data on specimens (repositories, accession numbers, stratigraphic ages, geographic ranges, body size, discussion on localities, body size inference of *Llanocetus denticrenatus*, and relevant literature), the character states and matrix used in the phylogenetic analysis. Moreover, in Supplementary File 1, links to the research results of the Paleobiology Database are provided in order to show the outputs of our searches in formats generated by the Paleobiology Database itself. In the Supplementary File 2, we provide the dataset compiled for the analysis of body size change in each mysticete family-rank taxon; the dataset is provided in a format readable by PAST (Hammer et al., 2001) and must be opened from within the PAST environment. The same data are also reported in Word in the Supplementary File 1 and can be read outside the PAST environment.

2.2. Phylogenetic analysis

We realized a new phylogenetic analysis of Mysticeti including 367 morphological characters scored for 98 Operational Taxonomic Units (hereinafter: OTU). The characters were mainly osteological and the character list is provided in Table S1 (Supplementary File 1). Currently, this is the most inclusive phylogenetic analysis of Mysticeti ever attempted up to now. The character x taxon matrix is presented in Table S2 (Supplementary File 1). The dataset was assembled based on the specimens listed in Table S3 and on the literature provided therein (see also Table S4 for institutional abbreviations used throughout the paper; Supplementary File 1). We used TNT

(Goloboff and Catalano, 2016) for phylogenetic inference. We used commands to hold 5000 cladograms in memory and then we performed 2000 random addition sequences of tree bisection reconnection algorithm (hereinafter: TBR) as implemented in TNT with 10 trees saved per replication. We assessed the morphological support at nodes by bootstrap (1000 replicates) and symmetric resampling (absolute frequencies; 33 change probability; 1000 replicates). A strict consensus (Nelsen) tree was calculated by TNT based on the most parsimonious cladograms found by the analysis. Both Consistency (CI) and Retention (RI) indices were calculated by TNT; the Homoplasy Index (HI = 1 - CI) was calculated by hand. To visually assess the number of supporting synapomorphies at nodes, we computed a phylogram using MESQUITE 3.61 (Maddison and Maddison, 2019).

Finally, to assess the agreement between the branching pattern of the phylogenetic result and the stratigraphic ages of the OTUs, we calculated the Stratigraphic Consistency Index (SCI) that is defined as (number of stratigraphically-consistent nodes)/(expected total number of nodes) (Huelsenbeck, 1997; see also Bisconti, 2007 for a discussion of pros and cons of using this index in mysticete phylogenetics).

2.3. Assessment of clade ages

Stratigraphic distributions of the mysticete taxa are provided in Table S3 (Supplementary File 1); the ranges in the table are used to realize Fig. 1 that will help to visualize the temporal abundance of mysticete species. It must be remarked that most of the past diversity of mysticetes is represented by species known only by one specimen (the holotype). In these cases, the stratigraphic distribution corresponds to the error of the estimation of the geological age of such a specimen. In those cases in which more specimens are known for the species, the stratigraphic distributions correspond to First Appearance Data (FAD) and Last Appearance Data (LAD) in the classical meanings of these terms. Various methods have been developed to statistically assess the minimum and maximum stratigraphic age of a clade based on its fossil record (reviewed by Wang and Marshall, 2016;

Rivadeneira et al., 2009). Statistical analyses rely on models describing the expected distribution of the fossil record and the diversification trends of the taxa under investigation (Wang and Marshall, 2016 and literature therein). Gingerich and Uhen (1998) discussed the models that could be applied to a statistical analysis of the time of origin of the Cetacea in great detail and observed that some of the models necessary for the application of a number of statistical equations have to be relaxed in order to get a thorough analysis of the cetacean fossil record. In particular, they discussed the applicability of the equation of Strauss and Sadler (1989) to determine the timing of the origin of Cetacea based on the stratigraphic assessment of the fossil record of the Archaeoceti, Mesonychidae and Hapalodectidae. The equation is based on an assessment of the Observed Temporal Density (OTD, that is the temporal range of a given taxon as documented by its fossil record and quantified by the time of its first and last appearances in the stratigraphic record), the Expected Temporal Density (ETD, that is the temporal range in which we expect to find fossils of a given taxon), the number of localities independently sampled in which fossils of the investigated group are found (n) and a probability level (λ) that can be set at 0.05 in order to have a statistically significant estimation of the time of origin. Equation (1) represents the Strauss and Sadler (1989) equation:

$$(1) \qquad \lambda = \left(\frac{OTD}{ETD}\right)^{n-1}$$

By resolving Equation (1), the ETD of a group can be inferred as follows:

$$(2) \qquad ETD = \frac{OTD}{\sqrt[n-1]{\lambda}}$$

where OTD is the observed temporal range obtained by the fossil record, n is the number of the localities where the fossils were independently sampled and λ is the level of statistical significance ($\lambda = 0.05$). Equation (2), thus, provides an estimation of the timing of origin of a taxon based on its observed temporal range as drawn from the stratigraphic ages of its fossil record in the sampled localities. Following the mathematical implementation of this formula by Gingerich and Uhen

(1998), the assumption of a uniform distribution of the fossils throughout the ETD can be ignored as we are interested in determining the timing of origin of a group and not its whole time span. Here, our purposes are to determine the time of origin of Chaeomysticeti, Balaenomorpha, Thalassotherii, basal thalassotherians, Cetotheriidae, Balaenoidea, Balaenidae, Neobalaenidae, Balaenopteroidea, Eschrichtiidae and Balaenopteridae (Table S5). We downloaded the stratigraphic data from the Paleobiology Database by searching for these groups (see paragraph *2.1. Structure of the dataset*). The time of first occurrence and the time of last occurrence (respectively: FAD and LAD for species known based on more than one specimen, and lower and higher limits of the error of estimations of the geological ages of species represented by the holotype only) of the taxa were computed (Table S3) and then the equation (2) was resolved in order to provide an estimation of the time of origin of each of the investigated clades. The ages of all the taxa used in the phylogenetic analysis are provided in Table S3.

2.4. Rates of morphological evolution

We used MESQUITE 3.61 to find the morphological transformations at nodes. We counted the maximum number of transformations for each node and then divided this number by the estimated duration of the ramus connecting the clade under investigation and the ancestor shared with its closest sister group in order to get an estimation of the mean number of morphological transformations per million years. Our phylogenetic analysis used an ACCTRAN optimization algorithm; following Brusatte et al. (2011), both ACCTRAN and DELTRAN algorithms provide similar morphospaces, therefore, the choice of one or the other is not strictly relevant to our goals. We then realized a histogram showing the cumulative number of morphological transformations detected in all the investigated lineages in order to find time intervals of accelerated or reduced morphological evolution.

We did not include autapomorphies in our dataset. We are aware that the autapomorphies play an important role in determining rates of morphological evolution but our work focuses on the origin

and evolution of main mysticete clades and not on single species, therefore the role of autapomorphies would not provide crucial detail in our analysis, justifying our decision to exclude them. To corroborate this point, we follow the results of Smith et al. (2021) who, in their analysis of disparity patterns, found that the internal branches of a cladogram characterize synapomorphic character evolution and predict the dispersal of taxa within the morphospace. On the contrary, terminal branches express the evolution of autapomorphies, predict the margin of the morphospace in which terminal taxa will diverge and increase the length of the terminal branches (Smith et al., 2021; Matzke and Irmis, 2016). We are interested in the origin of main mysticete clades and, therefore, the distribution of synapomorphic characters across internal nodes is our focus. As autapomorphies play no role in this kind of research, we did not include autapomorphies in our dataset.

To better visualize the distribution of synapomorphies at the internal nodes of the cladogram, we realized a phylogram by using MESQUITE 3.61. In the phylogram, the length of each ramus is proportional to the number of the inferred morphological transformations.

2.5. Rates of body size change

Bisconti et al. (2021) analyzed the evolution of body size in right and bowhead whales (Balaenidae) and provided a rationale to define different size classes for mysticete whales. Their rationale represents a synthesis of morphometric and physiological works resulting from different research strategies (e.g., Goldbogen et al., 2019; Marx et al., 2019; Slater et al., 2017; Fordyce and Marx, 2018). We adopted the following definitions provided by Bisconti et al. (2021): small-sized species, body length < 8 m; medium sized species, body length between 9 and 13 m; large-sized species, body length between 14 and 20 m; and gigantic species, body length > 20 m. Bisconti et al. (2021) justified the restriction of the term ‘gigantic’ to only species with total body length (hereinafter, TL) > 20 m based on the observations of Goldbogen et al. (2019) that only three of the extant species (i.e., *Balaenoptera musculus*, *Balaenoptera physalus* and *Megaptera novaeangliae*) may attain

more than 20 m in TL thanks to peculiar abilities to engulf enormous quantities of high-energy prey. These three species are among the largest animals that ever lived in our planet (Slater et al., 2017; Pyenson and Sponberg, 2011).

Our assessment of TL in extinct mysticetes is largely based on the results published by Bisconti et al. (2021) and Slater et al. (2017) for the Balaenoidea and the other non-balaenoid mysticetes, respectively. Taxa that were not assessed in these works but that are included in the present study are non-balaenoid ones and their TL is assessed herein by applying the formula provided by Slater et al. (2017) for stem-balaenopterids. The TL of the taxa included in the present work are provided in Table S6 (Supplementary File 1).

To quantitatively assess the rate of TL change across the mysticete phylogeny, we reconstructed the TL at ancestral nodes by maximum parsimony inference as implemented in MESQUITE 3.61. Changes occurred in TL in the different mysticete families were represented by box plots vs time. Our study of body size evolution in mysticetes is not based on an *a priori* assumption of linear variation through time. The distribution of TL values through time is the only datum on which we make observations and analyses.

2.6. Diversity change throughout mysticete evolution

The diversity (in terms of species number) of mysticete clades was graphically assessed by plotting the number of species present in time bins of 0.5 Ma based on the fossil record and on cladistic results. We analyzed the mysticete species known in the fossil record from data downloaded from the Paleobiology Database and available from Supplementary File 2. Assessments of extinction and origination rates were performed by plotting the number of earliest and latest occurrence of taxa (based on LAD and FAD of species represented by more than one specimen, and on lower and upper limits of the error of the estimation of the geological ages of species represented by the holotype only) vs time in time bins of 1 Ma. Finally, the diversity of different families was plotted vs time to realize a sort of illustration of ‘evolutionary faunas’ in the sense of Sepkoski et al. (1981;

see also Droser 2003) to help visualizing possible competitive relationships between families. As usual, in the case in which the diversity of a single family declines at the same time when that of another family increases, then a process of competition-driven extinction is observed. We plotted both the actual fossils depicting the diversity of known families and clades based on our phylogenetic results vs time.

2.6. Relationships to Cenozoic global changes

Patterns of body size and morphological evolution were compared with published geochemical, paleontological and sedimentological proxies of paleoclimatic and paleoceanographic changes occurred throughout the Cenozoic, with the aim of highlight possible relationships. Particular attention has been given to planktic diatoms (Bacillariophyceae), i.e. silica-shelled unicellular primary producers at the base of the marine trophic chain on which mysticetes rely (e.g., Kooistra et al., 2007), and to the abiotic and biotic factors that controlled their abundance from the Eocene onward.

3. Results

3.1. Revisions of localities

We checked more than 1400 localities for fossil mysticetes that are reported in the Paleobiology Database. The localities are provided in the dataset published online in the Supplementary File 3. We dismissed some localities following specific discussions as reported in the notes to the Table S5 (Supplementary File 1).

3.2 Phylogenetic analysis

The results of the phylogenetic analysis are shown in Fig. 2 where the strict consensus of 26 most parsimonious cladograms is presented. The most parsimonious solution is 1991 steps in tree length;

it has a Consistency Index (CI) of 0.247, a Retention Index (RI) of 0.736 and an Homoplasy Index (HI) of 0.753.

The present analysis recovers Mysticeti as a monophyletic group. Earliest diverging mysticetes are the Mammalodontidae, followed by *Fucaia* and *Aetiocetus* representing the most plesiomorphic, toothed mysticetes known up to now. A clade formed by *Llanocetus*, *Maiabalaena*, *Toipahautea*, *Mystacodon* and *Coronodon* is detected here for the first time and is referred herein to as *Maiabalaena*-like group. This clade is the sister group of *Tohoraata raekoao* that is, in turn, the sister group of the Chaeomysticeti (including all the baleen-bearing mysticetes). The Eomysticetidae are the basal-most chaeomysticetes and represents the family-rank group that is closer to Balaenomorpha (including all the extant mysticete families). Interposed between Eomysticetidae and Balaenomorpha are two Oligocene taxa, *i.e.*, *Sitsqwayk cornishorum* and *Horopeta umarere*. *Sitsqwayk* is the sister group of the Balaenomorpha.

Balaenomorpha is split into two large monophyletic groups: Balaenoidea (including Balaenidae and Neobalaenidae) and Thalassotherii (including basal thalassotherian taxa, Cetotheriidae and Balaenopteroidea). The basal thalassotherian taxa are recognized as monophyletic herein and form a family-rank clade that still has to receive a formal denomination. Several subgroups of basal thalassotherians are detected and could represent distinct subfamilies but we abstain from providing new names as additional comparative information is necessary to further test the long debated monophyly of this group. *Taikicetus* is the sister group of Cetotheriidae + Balaenopteroidea (including Eschrichtiidae and Balaenopteridae). Eschrichtiidae is a monophyletic group excluded from being part of Balaenopteridae.

Bootstrap support values and symmetric resampling values (shown in Fig. 2) show support for most of the main mysticete clades described above. In particular, strong support is found for the monophyly of the Mysticeti, Balaenomorpha, Balaenoidea, Eomysticetidae, Balaenidae and Neobalaenidae. In the present analysis, the other family-rank clades received less than 50% from both bootstrap and symmetric resampling. Low bootstrap supporting values may depend on several

factors. In particular, bootstrap values are inversely proportional to (1) number of characters of the dataset, (2) number of autapomorphies, (3) number of non-informative character states for a given node, and (4) increased taxon sample. In our dataset, both the taxonomic and morphological samples are quite high thus leading to reduced bootstrap supporting values. A certain degree of homoplasy, as testified by CI, RI and HI, together with question marks in the matrix certainly contributed to lower the bootstrap supporting values.

Additonal >50% supporting values are found for the monophyly of *Atlanticetus*, *Echrichtius* + *Eschrichtioides*, *'Balaenoptera' cortesii* var. *portisi*, *Protororqualus* and *Incakujira*. Other relationships are too poorly supported by bootstrap and symmetric resampling and the corresponding values are not shown in Fig. 2.

A schematic representation of the relationships of the family-rank clades is shown in Fig. 3. Most of the mysticete taxa known from the extant and the fossil record are included in a minimum of eight family-rank clades, some of which still need to be denominated. A few species still fall outside the family-rank clades including *Fucaia*, *Tohoraata*, *Horopeta*, *Sitsqwayk* and *Taikicetus*. These taxa cannot be assigned to new families as additional morphological information is necessary to better characterize most of them.

3.3. Chronology of main mysticete clades

We used the OTR values in Tables S3 and S5 to resolve Equation (2) for mysticete clades. The results are shown in Table 1 where OTR, ETR and observed and estimated clade stratigraphic ranges (respectively, OCSR and ECSR) are presented. The origin of Mysticeti is traced back to 38 Ma in the late Eocene; the time of origin of Chaeomysticeti is estimated being *c.* 34 Ma (latest Eocene-to-earliest Oligocene) suggesting that the origin of filter feeding occurred very quickly after the origin of the mysticete body plan. The origin of Balaenomorpha is estimated *c.* 23.3 Ma at the beginning of the Miocene when all the main crown mysticete clades (i.e., Balaenopteroidea, Balaenoidea and Thalassotherii) occur in the fossil record.

We estimated also the time of origin and stratigraphic durations of family-rank taxa including Eomysticetidae (ECSR: 29.2-20.4 Ma), Thalassotherii (ECSR: 23.11-0 Ma), Cetotheriidae (19.8-0.8 Ma), basal thalassotherian taxa (ECSR: 24-7.1 Ma), Balaenopteroidea (ECSR: 20-0 Ma) and Balaenopteridae. The ECSR of these clades allowed to infer clade durations (Table 1) that were used for the calculus of rates of morphological and size change.

We plotted the simplified version of the mysticete phylogeny of Fig. 3, including only family-rank taxa, against a time scale and presented the result in Fig. 4. Four main diversification events are detected from our chronological reconstructions. We named these events with Greek letters and numbers following the scheme proposed by Bisconti et al. (2019). Our results suggest that the first event of Bisconti et al. (2019) is to be splitted into two different events. In fact, while in Bisconti et al. (2019) resolution was too low to unravel the structure of the first event (α event of Bisconti et al. 2019), here we performed a more detailed analysis that allowed us to dissect this event and find that it is actually formed by two distinct sub-events. We decided to maintain the names of the main events as provided by Bisconti et al. (2019) and designed two sub-events deriving from the splitting of the α event (α_1 and α_2). The first, α_1 represents the origin of Mysticeti; the second, α_2, represents the origin of the Chaeomysticeti.

This reconstruction implies that the process of assembly of the chaeomysticete characters occurred in *c.* 10 million years and that additional stem-Chaeomysticeti are expected to occur in the time interval between 34 (inferred origin of Chaeomysticeti) and 28 (origin of chaeomysticete whales such as Eomysticetidae) Ma.

The β event in the late Chattian (late Oligocene) represents the origin of Balaenomorpha or crown mysticetes. It marks the divergence between the Balaenoidea and the Thalassotherii, and represents a major event in that two different filter feeding groups, characterized by profoundly different feeding styles, diverged from a common ancestor: the continuous ram feeders (Balaenoidea) and the intermittent ram feeders (including extant Balaenopteridae and, possibly, both basal Thalassotherian taxa and Cetotheriidae). By implication, it is expected that the stem-Thalassotherii were in existence

from the inferred divergence time corresponding to the β event even in the absence of fossil evidence, as the earliest fossil thalassotherians date back to the Burdigalian, early Miocene (*c.* 20 Ma), about 4 million years after the inferred divergence time from the common ancestor shared with Balaenoidea.

The γ event corresponds to the splitting of Thalassotherii into three different clades: basal thalassotherian taxa, Cetotheriidae and Balaenopteroidea. It occurred approximately at the Aquitanian/Burdigalian boundary around 20 Ma. The Cetotheriidae originated from its sister group during the γ event. *Protororqualus dyticus* (Cabrera, 1926) from the early Miocene of Argentina marks the early origin of Balaenopteroidea (according to Bisconti and Bosselaers, 2021) in the γ event.

Bisconti et al. (2019) designated the δ event occurred at the transition between Langhian and Serravallian in the middle Miocene (*c.* 14 Ma) as marking the origin of Balaenopteroidea and the divergence of Eschrichtiidae and Balaenopteridae. Our analysis supports the view that the origin of Balaenopteroidea is part of the γ event and for this reason we labeled the γ= δ event in Fig. 4. Therefore, the δ event of Bisconti et al. (2019) is abandoned here.

3.4. Patterns of extinctions and originations

In Fig. 5, we show the diversity of mysticetes based on fossil occurrences (Fig. 5A) and inferred clade presence (Fig. 5B). Both graphs show approximately the same pattern that can be summarized as follows: (i) an early phase of diversity expansion that started in the Priabonian and ended at the end of the Chattian; (ii) a phase of reduced diversity in the stratigraphic interval in the Aquitanian; (iii) a new phase of diversity increase from the Burdigalian to the end of the Pliocene punctuated by additional events of diversity loss and increase. In Fig. 5B, clade diversity abruptly increased *c.* 9 Ma and dropped again around 7 Ma. In both graphs the origin of the modern mysticete species is part of a process of diversity increase.

Increases and decreases of diversity are analyzed in light of origination and extinction patterns in Fig. 6 on scale of 1 million years. In the earliest phases of mysticete existence, originations are scattered along a time interval of *c.* 10 million years between the Priabonian and the Chattian when scarce extinction events are recorded in both the fossil record and clade durations. Evident extinction pulses in this phase are observed between 29 and 23 Ma. This pattern may help to explain the diversity fall observed in the Aquitanian as shown in Fig. 5A,B. Interestingly, this pattern shows that when the earliest mysticete morphotypes went extinct, they were not replaced by new species in the same clades. Rather, the extinct species created vacant niches although it is unlikely that these niches were occupied by chaeomysticetes as the feeding styles of the latter were very different from those of the earliest mysticetes. The key morphological synapomorphy of Chaeomysticeti, in fact, is the presence of baleen (Bisconti and Carnevale, 2022) that allows the performance of filter feeding in contrast to the earliest mysticetes that used a combination of biting and suction to mainly prey upon fishes (Berta and Lanzetti, 2020). Possible overlap in feeding styles could have been present between the archaic, toothed-mysticetes and the chaeomysticetes in the case in which the coexistence of teeth and baleen would be definitely accepted in Aetiocetidae (as proposed by Deméré et al., 2008 and reiterated by Ekdale and Demeré, 2021; and Gatesy et al., 2022). However, alternative hypotheses have been formulated, which must be further corroborated by convincing morphological evidence (e.g., Peredo et al., 2021, 2017; Hocking et al., 2017; Marx et al., 2016), excluding the possibility that teeth and baleen coexisted in the same species.

Starting from the Aquitanian/Burdigalian boundary, intense origination events are observed that occur at the same time as a number of extinction events. This is the common pattern observed in the stratigraphic interval between Burdigalian and today, and corresponds to one of the main diversity increases represented in Fig. 5A,B (γ event of Fig. 4). Higher rates of originations are observed between 15 and 12 Ma, 10 and 7 Ma, and between 4 and 2 Ma. Higher extinction rates are observed between 8 and 7 Ma, and 4 and 2 Ma. This origination/extinction pattern is also evident from Fig. 7, where the mysticete phylogeny presented in Fig. 2 is plotted against a time scale including data for

originations and extinctions of each taxon based on Table S3 (Supplementary File 1). In this graph, the extinctions of the earliest, toothed mysticetes group occurred in the middle-to-late Oligocene and no branches overcome the Oligocene-Miocene boundary, as also observed in Fig. 5A,B. There is an overlap of stratigraphic ranges of toothed-mysticetes and earliest chaeomysticetes during the late Oligocene; the stratigraphic ranges of *Sitsqwayk* and *Horopeta* demonstrate that also the stem-Balaenomorpha were present in the late Oligocene. The origin of Balaenomorpha is thus to be searched in the mid-to-late Oligocene. Judging from Fig. 7, stem-Balaenomorpha are expected to originate in the latest Rupelian (early Oligocene). The complete assembly of the synapomorphies of Balaenomorpha required *c.* 6 Ma and took place between 34 and 28 Ma (Fig. 7).

The Miocene was the period with maximum mysticete diversity. Both the graphs in Fig. 5A,B and 7 show that Balaenomorpha was a successful clade and that most of the known species were existent in the stratigraphic interval between Burdigalian and Tortonian. While there may be some sampling bias due to inadequate fossil record in Aquitanian and Messinian stages, the number of localities in which fossil mysticetes have been found corresponds to several hundred in the Aquitanian-Messinian interval, suggesting that the available information may be regarded as a reliable biological evidence. In this respect, Marx et al. (2019; see also literature therein) observed that there are several worldwide formations in which Aquitanian strata crop out that are rich in odontocete fossil remains but that bear a few or no mysticete fossils at all. The abundance of Aquitanian odontocetes rules out taphonomic artifact or significant sampling bias about the abundance assessment of Aquitanian mysticetes from the known localities. Marx et al. (2019) suggested that Aquitanian mysticetes (mainly belonging to Chaeomysticeti) moved offshore rather than remaining inshore as the pre-existent toothed mysticetes, and this prevented abundant fossilization due to the sedimentary and biotic characteristics of the oceanic floor in which complete destruction of whale skeletons is largely documented (see Dominici et al., 2020 for an extensive review of this process and further literature). This hypothesis could explain why aquitanian mysticetes are rare. In any

case, it is apparent that Aquitanian localities are less numerous than localities from better sampled time intervals and, therefore, a source of bias may still be present.

Several species went extinct at the Piacenzian/Gelasian boundary (*c.* 2.6 Ma) representing the end of whole lineages (e.g., stem-balaenopterids) that were highly represented in the late Miocene and Pliocene. The origination pulse observed in the Pleistocene in Fig. 5A,B and Fig. 7 is due to the origin of the modern mysticete fauna (begun in the latest Miocene), including the genera *Balaenoptera* and *Megaptera*, *Eschrichtius* and the extant right and bowhead whales (*Eubalaena glacialis*, *E. australis*, *E. japonica* and *Balaena mysticetus*).

3.5. Evolutionary faunas

We investigated the taxonomic composition of the mysticete diversity through time to understand the proportional contribution that each family-rank clade provided to the global diversity pattern. Our result is shown in Fig. 8. Both fossils (Fig. 8A) and branching pattern (Fig. 8B) show diversity peaks and valleys consistent with the events described above. In the curves of Fig. 8, different colors quantitatively represent the numbers of species belonging to each family-rank clade and show the relative proportion of each of these clades during time intervals of 0.5 million years.

The initial diversification event of the mysticetes begun about 38 Ma with the early evolution of toothed mysticetes; toothless and baleen-bearing mysticetes originated quickly after the initial divergence of Mysticeti and maintained a comparable diversity with that of toothed taxa up to *c.* 23 Ma. No evident pattern of competition is observed in this phase (38-23 Ma) as toothed and baleen-bearing mysticetes underwent similar diversification paths. An important extinction event occurred at the Oligocene/Miocene boundary, *c.* 23 Ma, which affected both toothed and baleen-bearing taxa; such an event was already recognized by Marx et al. (2019) and was evident in the analysis of the mysticete diversity of Bisconti et al. (2019).

The clade-based analysis of diversity, shown in Fig. 8B, suggests that the earliest Balaenomorpha originated toward the end of the Chattian (β event) even though the fossil record documents their

presence only from the Aquitanian (see Fig. 8A in which the β event is not recorded), with their radiation that took place during the process that led toothed-mysticetes to the extinction. It is still unclear whether the origin of Balaenomorpha triggered a competitive mechanism able to drive earliest mysticetes to disappear or not. More evident competitive patterns are observed in subsequent phases and will be discussed below.

The γ event is mainly due to the expansion of the diversity of basal thalassotherians in the Burdigalian and Langhian; all the other balaenomorh families marginally contributed to the total diversity in the stratigraphic interval between 20 and 16 Ma. Starting from *c.* 16 Ma, there is an increase in the diversity of Cetotheriidae that parallels a contemporaneous fall of the diversity of the basal thalassotherians. The relationship between the increase in cetotheriid diversity and decrease in basal thalassotherian diversity is evident from both fossil-based and clade-based analyses (Fig. 8A,B). This observation suggests an overlap in ecological preferences by these two family-rank clades.

The rise of the Cetotheriidae was concluded when an expansion of the balaenopteroid diversity occurs beginning from *c.* 13 Ma. The quick increase of balaenopteroid diversity sharply parallels the fall of cetotheriid diversity and the extinction of the basal thalassotherian taxa *c.* 8 Ma. Such an extinction occurred during the event 2 of Bisconti et al. (2019) in which the maximum balaenopterid diversity is attained. Competitive mechanisms are evident from these curves suggesting overlap between the ecological preferences of Balaenopteridae, Cetotheriidae and basal thalassotherian taxa. Balaenopterids maintained a dominant contribution to the taxonomic composition of the mysticete diversity through the whole Neogene with another pulse in diversity (event 3: Pliocene) up to today. Interestingly, the clade-based analysis shows that the balaenid diversity remained nearly constant through the last 23 million years with moderate peaks in the late Miocene and Pliocene.

Bisconti et al. (2019) distinguished three diversification events of Balaenopteridae (see also Fig. 8). The first event (No. 1) corresponds to the early diversification phase of basal rorquals. The second

event (No. 2) corresponds to a Tortonian peak in mysticete diversity that is mainly due to a massive expansion of balaenopterid diversity; this peak is recognized as one of the most important diversification events in the history of mysticetes (Berta and Lanzetti, 2020; Bisconti et al., 2019; Marx and Fordyce, 2015; Marx and Uhen, 2010). The third event (No. 3) corresponds to a Pliocene peak in diversity attained by both Balaenopteridae and Balaenidae recognized also by Berta and Lanzetti (2020) and Marx and Uhen (2010).

3.6. Rates of morphological evolution

All the character state changes were reconstructed by MESQUITE that allowed inference of character states at ancestral nodes. We counted all the unambiguous character state changes along selected branches in the phylogeny of Fig. 3 representing family-rank taxa and species that cannot be included within any of the known families based on the phylogeny of Fig. 3. The changes were subdivided by the duration of the branch as reconstructed from Table 1 and Figs. 4 and 7. The results are presented in Fig. 9. We observed three different patterns: (1) the origin of the Mysticeti was marked by a high number of morphological changes in a relatively short period of time (we detected 22 morphological changes in 3 million years: 7.33 changes per million years); (2) the transition from earliest, toothed mysticetes and chaeomysticetes was slow and gradual (6 morphological changes in 8.9 million years: 0.67 changes per million years); (3) the period between 28 and 14 million years was characterized by high rates of morphological changes. The latter observation is consistent with the time constraints for the origin of Balaenomorpha (5.94 changes per million years), Thalassotherii (4.31 changes per million years), Cetotheriidae (4.44 changes per million years) and Balaenopteroidea (7.77 changes per million years).

The rates described at point (3) occurred at the period in which the earliest-, toothed mysticetes and Eomysticetidae decreased in diversity and eventually became extinct, and the origin of Balaenomorpha and its subdivisions (Balaenoidea and Thalassotherii) occurred (Fig. 5). The high number of extinction events occurring between 29 and 23 Ma and the high number of originations

occurring between 21 and 16 Ma (Fig. 6) suggest that an intense selective regime was acting on mysticetes, during the time interval between 29 and 14 Ma, favoring the divergence of the main balaenoid and thalassotherian branches and the origins of the principal feeding styles of mysticetes.

3.7. Body size evolution

We analyzed the distribution of body size in all the mysticete taxa investigated along their stratigraphic ranges. We recorded all the body sizes of the species in time intervals of one million years. The resulting box plot is shown in Fig. 10. Our analysis shows that mysticetes had small body sizes (TL included between *c.* 4 and *c.* 9 m) for most of their evolutionary history. In particular, toothed mysticetes were small-sized and never evolved medium-to-large size (this includes the holotype of *Llanocetus* whose TL does not exceed 9 m; we were unable to replicate the TL=12 m for the *Llanocetus* sp. specimen IAA Pv 731 based on the formulae used by Marx et al., 2019; our results range between 3.7 and 4.6 m for this specimen: see Supplementary Online Material Text S1). As shown in Fig. 10, a TL longer than 10 m is hardly observed in mysticetes before the early Tortonian (*c.* 10 Ma), which is still consistent with the observation of a more than 10 m long putative *Pelocetus* specimen still in the field in the Peruvian Pisco Formation, cursorily reported by Bianucci et al. (2019). Interestingly, rather than observing a clear trend toward longer TL values, our analysis shows a trend toward an expansion in body size range for mysticetes in the interval between Langhian and present. Pulses of increase in body size range are observed in the Langhian, Tortonian and Pliocene. The maximum increase in body size range is observed in the latest Pliocene and in the Pleistocene, with a neat drop in the last million year probably following the general trend toward diversity decrease observed in Fig. 8. In more recent times, the gigantic blue and fin whales (*Balaenoptera musculus* and *B. physalus*) represent outliers whose maximum TL values are not included within the main range of variation of extant mysticete species. This is consistent with the model elaborated by Goldbogen et al. (2019) on the hypothesized metabolic path able to drive the evolution of gigantism in mysticetes suggesting that gigantic body size (i.e., TL >

20 m) should be considered as an exceptional output of an evolutionary lineage rather than the normal *status quo*.

Interestingly, our data suggest that the temperature decrease of the Pleistocene did not impact mysticete biology in only one sense (i.e., evolution of gigantic TL values); rather, during Pleistocene, we observe an increase in the TL range suggesting evolution of different ecological strategies and, possibly, occupation of more ecological niches. This is particularly evident in the rorquals of the North Atlantic that have different alimentary specializations (see reviews in Barros and Clarke, 2002; Kawamura, 1980) and in the geographic differentiation of right and bowhead whales. More detailed analysis of the morphological changes occurred in the Plio-Pleistocene are necessary to test this hypothesis but this is beyond the scope of the present paper.

Based on the operational definition of gigantism, we observe that gigantic size occur only in Balaenopteridae and Balaenidae. All the other mysticete taxa were small-to-middle sized (Supplementary Fig. S3). The first increase in body size range is contemporaneous with the early appearance of the basal thalassotherian taxa in the early Langhian following a period characterized by high rate of morphological change (Fig. S1 in Supplementary File 1). A slight increase in mean TL is observed in Tortonian (mean TL is *c.* 5 m) and Messinian (mean TL is *c.* 7 m) (Fig. 10). Subsequently, a slight change in mean TL is observed in the early Pliocene (mean TL is *c.* 6 m); an abrupt increase in the mean TL is observed starting from the earliest Pleistocene (mean TL is *c.* 10 m). The smallest mysticetes (TL < 5 m) disappear from the fossil record starting from the Calabrian, in the middle Pleistocene.

Family trends are shown in Figs S1-S3 (Supplementary File 1). The graphs show that different trends occurred in different families. Among the earliest mysticetes, in the time interval between 28 and 25 Ma, we observe that the eomysticetids and Aetiocetidae increased their TL, although *Maiabalaena*-like taxa decreased TL values suggesting that a process of niche partitioning possibly took place. In the time interval between 16 and 10 Ma, we observe an early TL increase in the basal thalassotherian taxa but a subsequent drop in TL values around 12 Ma when the Cetotheriidae

started increasing TL values. The same observation is made for the time interval between 9 and 2 Ma when the TL reduction in the Cetotheriidae occurred with the TL increase occurring in the Balaenopteridae. The last cetotheriids (*Herpetocetus* sp.; Boessenecker, 2013) had the smallest size of all Cetotheriidae and were living side to side with large balaenopterids (Fig. S2).

The maximum mysticete diversity was attained during the middle Miocene and is characterized by an expansion in the body size range that included small-, medium-, and large-sized species (Fig. S1); this pattern is observed up to the early Pliocene when small and medium-sized mysticetes are the only ones present in the fossil record but large- and gigantic-sized species are absent. A new expansion in TL range with evolution of small-, medium-, large-, and gigantic-sized species starts from the beginning of Pleistocene and leads to the present time (Fig. S2).

We reconstructed the most likely size at the ancestral nodes of the phylogeny shown in Fig. 2 using the maximum likelihood algorithm of MESQUITE, which are shown in Fig. 11. We observe that most of the TL values for extinct mysticetes fall in the small-sized category; medium, large and gigantic sizes evolved independently in several lineages. The large size of the Tortonian balaenopterid MuMAB 240508 is interpreted as an early and independent evolution of large body size in an archaic, early balaenopterid. Interestingly, in the time interval comprised between Langhian and Tortonian, a number of mysticetes evolved a medium size; these include *Uranocetus gramensis*, *Pelocetus calvertensis*, *Archaeschrichtius ruggieroi*, *Norrisanima miocaena* and *Plesiobalaenoptera quarantellii*. Interestingly, eschrichtiids appear to have been medium-sized since their origin. A trend toward increasing TL values is observed in the Balaenopteridae starting from the Tortonian (*Norrisanima miocaena*) up to today, although a trend in miniaturization that involved the origin of the extant minke whale (*Balaenoptera acutorostrata*) can be also observed. This is not surprising in the light of a hypothesis of a niche partitioning process during the last million years (Fig. 11). Gigantism is never observed as the unambiguous ancestral state for a mysticete clade even though a TL increase represents an ancestral character of a single rorqual clade (the one leading to the extant species of *Balaenoptera* and *Megaptera*).

3.5. Relationships to Cenozoic global change

The relationships between the patterns of body size and morphological evolution of mysticete cetaceans and Cenozoic global events, reported in Figs. 12-14, are discussed herein.

3.5.1. α1-3 events

The α1-3 events of mysticete diversification occurred around the Eocene/Oligocene boundary (ca. 39 to 28 Ma). During the E/O transition the climate changed from greenhouse to icehouse conditions, with the establishment of the first Antarctic glacial cover about 37 Ma (Zachos et al., 2001; Fig. 12). The global average temperatures dropped from ca. 24°C (Middle Eocene Thermal Maximum; Scotese et al., 2022; Fig. 12) to ca. 15°C (major drop of the Late Eocene-Oligocene Cooling; Scotese et al., 2022; Fig. 12). At the same time, remarkable turnovers occurred in terrestrial ecosystems, where grasses started to spread, probably favored by a concurrent intensification of the fire regime (Strömberg & Staver, 2022; Fig. 13). Major tectonic events during this period include the onset of the Alpine-Himalayan orogeny (Cermeño et al., 2015; Fig. 13), as well as the opening of the Drake and Tasmanian passages, which initiated the isolation of the Antarctic landmass and the establishment of the Proto-Antarctic Circumpolar Current (Potter & Szatmari, 2009, 2015; Sarkar et al., 2019; Fig. 13). Significant volcanic activity is recorded in Africa, associated with the Hoggar volcanism, the eruption of Ethiopian traps and the initial Red Sea and East African rifting (Rognon et al., 1983; Aït-Hamou et al., 2000: Couvreur et al., 2020; Boone et al., 2021; Fig. 13), in America (Basin and Range and Great Basin volcanism; Sternai et al., 2021; Fig. 13), and in Iceland, with a marked increase of the magmatic flux (Døssing et al., 2016; Fig. 13). Although the sediment yield decreased during the α1-3 events, the occurrence of an active weathering in continental settings is suggested by Sr isotopes, which show a slight but continuous increase from the α1 event onward, and by the dissolved Si flux, which peaked around

the α3 event (Fig. 12). Intriguingly, the α2 event coincided with the most significant phosphogenetic event recorded in the Cenozoic (e.g., Hyeong et al., 2013). Diatom productivity raised shortly after the α-2 event, as well as diatom diversity, both accompanied by a positive peak in $\delta^{13}C$ (Zachos et al., 2001; Renaudie, 2016; Fig. 14). Although during this period the diatomaceous production was mostly focused in the South Atlantic (Renaudie, 2016; Fig. 14), an explosive diversification and abundance increase of *Chaetoceros* resting spores is also recorded in the North Atlantic during the α-1 and α-2 events (Suto, 2006; Fig. 14), and a prolonged period of opal accumulation also occurred in the Southern Pacific (Sarkar et al., 2019; Fig. 14), in coincidence with the initial establishment of the Northern Component Water and of the Proto-Antarctic Circumpolar Current (Steinthorsdottir et al., 2021; Fig. 14). The E/O transition also recorded the rise of basal lanternfishes, which started to colonize the mesopelagic environment, slightly increasing their mean sizes at least from the α-1 to α-2 event (Schwarzhans & Carnevale, 2021; Fig. 14).

3.5.2. β event

The β event of mysticete diversification coincided with another drop in the global temperatures (Fig. 12). On lands, grasslands expansion continued at the expense of forests, with the appearance of the first grass-dominated ecosystems in North America (Strömberg & Staver, 2022; Fig. 13). The main tectonic and erosional events during this period were the closure of the Indonesian gateways, the Southern Cordillera uplift and a generalized uplift of Northern Europe and for a less extent of the Asian region, this latter favoring an increased siliciclastic deposition in the Mekong and Red River basins (Potter & Szatmari, 2009, 2015; Cather et al., 2012; Ollier & Pain, 2019; Fig. 12). Volcanism was mostly associated to the Great Basin Ignimbrites (Sternai et al., 2021; Fig. 13). Sediment input to the oceans was significantly higher than during the previous α events (Sternai et al., 2021) as well as Sr isotopes, although the Si flux from continents was less pronounced than

during the α-3 event (Renaudie, 2016; Fig. 12). Phosphogenesis persisted at rather high rates (Hyeong et al., 2013; Fig. 14). Diatom abundance was high at the beginning of this event, while diatom diversity increased at the end (Renaudie, 2019; Fig. 14). Remarkably, the β event coincided with another $\delta^{13}C$ rise, the so-called Oligocene-Miocene Carbon Maximum (Zachos et al., 2001; Steinthorsdottir et al., 2021; Fig. 12), with the first significant event of opal deposition in the Southern Ocean and in another peak of diversification of *Chaetoceros* resting spores in the North Atlantic (Suto, 2006; Fig. 14). The β event also recorded an increase of diversity of lanternfishes (especially of the very abundant genera *Diaphus* and *Lobianchia*), although slightly smaller in size than before (Schwarzhans & Carnevale, 2021; Fig. 14).

3.5.3. γ event

This event partly overlapped the Early Miocene Cooling Interval (Scotese et al., 2022; Fig. 12). Noteworthy, deserts started to expand in the Asian continental interior, as witnessed by the first remarkable spike of aeolian quartz in the detrital contribution to Pacific Ocean (Guo et al., 2002; Zheng et al., 2016; Fig. 12). During this period, the global rates of ridge spreading reached a minimum (Potter & Szatmari, 2009; Fig. 13), although Red Sea rifting went on (Boone et al., 2021; Fig. 13), the Hoggar volcanism increased (Rognon et al., 1983; Aït-Hamou et al., 2000; Fig. 13), uplift occurred in Europe (Pyrenees, Lake District, Peninnes; Ollier & Pain, 2019), and sediment yield and Sr isotopes continued to increase (Sternai et al., 2021; Renaudie, 2016; Fig. 12). Dissolved Si flux remained rather stable (although they may have decreased if considering the clay-based inference instead of the Li isotopes; Cermeño et al., 2015). According to Renaudie (2016), the early Miocene diatom productivity was rather scarce. Some new loci of diatomaceous deposition started to occur at the mid latitudes, probably in response to the onset of coastal upwelling cells (Renaudie, 2016; Fig. 14). Phosphogenesis persisted up to the initial part of this event, then drastically dropped (Hyeong et al., 2013; Fig. 14). Lanternfishes diversity expanded,

and their size increased again after the slight decrease occurred during the β event (Schwarzhans & Carnevale, 2021; Fig. 14).

3.5.4. 1, 2 and 3 events

From the middle Miocene onward, remarkable climatic, tectonic, ecological and oceanographic transitions occurred. Following the Mid-Miocene Thermal Maximum, global temperatures and sea level started to drop again, inaugurating the Late Miocene Cooling Interval and the Messinian Glaciations, a prelude to the subsequent Pleistocene glaciations (Haq et al., 1987; Scotese et al., 2022; Fig. 12). Ice-sheet appeared in the Northern Hemisphere (Zachos et al., 2001; Fig. 12). Increasing aridity led to the full establishment of flammable, grass-dominated ecosystems populated by hypsodont grazers (Strömberg & Staver, 2022; Fig. 13). Desert expanded in Southern and Central-North Africa and South America, and the dust contribution to detrital fraction significantly increased (Senut et al., 2009; Jordan et al., 2014; Schuster et al., 2006; Zheng et al., 2016; Fig. 1**3**). Tectonic activity (notably the Andean and Himalayan uplift; the closure of the Mediterranean to Atlantic gateways leading to the Messinian salinity crisis; Fig. 14), erosional processes (e.g., increased siliciclastic influx to North American, Indian and Asian basins) and volcanism (e.g., Columbia River Basalts; Fig. 14) were globally enhanced, likely in response to the reactivation of the African and Pacific superplumes (Potter & Szatmari, 2009, 2015; Fig. 14). A significant increase of sediment yield, Sr isotopes and dissolved Si flux occurred, particularly marked from the middle to late Miocene (Sternai et al., 2021; Renaudie, 2016; Fig. 12). Both diatom abundance and diversification underwent significant peaks, decreasing after the early Pliocene, especially at the low-to-mid latitudes (Renaudie, 2016; Fig. 14). With the firm establishment of the North Atlantic Deep Water in the middle Miocene, the thermohaline circulation assumed the present-day configuration. This lead to the so-called ‘silica switch’ from the Atlantic to the Pacific, i.e. a general nutrient impoverishment of the Atlantic Ocean and the shift of the main loci of opal deposition

along the Pacific upwelling cells, strengthened by the increased pole-to-equator thermal gradient (Keller & Barron, 1983; Barron, 2022; Fig. 14). Consequently, the enhanced shuttling of organic matter to the seafloor favored new community of sea-floor inhabitants, like benthic foraminifera adapted to exploit organic-rich substrates (Steinthorsdottir et al., 2021). Organic matter accumulation was particularly favored in semi-enclosed basins such as the Mediterranean, where sapropels started to accumulate at *c.* 13.5 Ma (Rohling et al., 2015; Fig. 13). Phosphogenesis resumed up to the early-to-mid Miocene transition (associated to the Monterey Event; Fig. 14), then dropped again and occurred significantly for the last time only during the Tortonian, in coincidence with a Carbonate Crash event (Steinthorsdottir et al., 2021). Nevertheless, a significant increase in P accumulation rate occurred during the late Miocene-early Pliocene in the Indian Ocean (Filippelli, 1997). This latter sedimentary event was associated to the so-called late Miocene-early Pliocene biogenic bloom, which consisted in a global increase of the marine biological productivity (Filippelli et al., 1997; Cortese et al., 2004; Pellegrino et al., 2018; Steinthorsdottir et al., 2021; Fig. 14). The biogenic bloom event was associated to the late Miocene carbon isotope shift (Steinthorsdottir et al., 2021) and to the global increase of giant diatom ooze deposition initiated at *c.* 14.5 Ma in the Eastern Equatorial Pacific (Kemp et al., 2006; Fig. 14). Noteworthy, the biogenic bloom was also associated to the radiation of deep dwelling planktic foraminifera (Boscolo-Galazzo et al., 2022; Fig. 14), as well as of tunas and other pelagic fishes (Santini et al., 2013; Santini & Carnevale, 2015). Both diversity and body size of lanternfishes underwent a significant increase (Schwarzhans & Carnevale, 2021; Fig. 14).

4. Discussion

4.1. Phylogenetic relationships of mysticetes

The morphological dataset used in the present paper is a modified version of previously used datasets by Bisconti et al. (2022, 2021a,b and literature therein). The results of the present phylogenetic analysis differ from those published in the above articles mainly because of the

inclusion of taxa and characters to resolve the relationships of basal mysticete taxa. We found a monophyletic clade including *Llanocetus, Toipahautea, Maiabalaena, Mystacodon*, and *Coronodon*, and we found that Mammalodontidae (including *Mammalodon* and *Janjucetus*) is the most basal mysticete clade. These results differ from other works published recent years by different research groups. For example, Geisler et al. (2017), in a phylogenetic analysis of *Coronodon*, found that Janjucetidae and Mammalodontidae formed a monophyletic clade and that *Llanocetus* is the sister group of Chaeomysticeti. These results were confirmed in large part by Lambert et al. (2017) who found that *Mystacodon* was the most basal mysticete instead of *Coronodon*. Interestingly, both the monophyly of Mammalodontidae and Aetiocetidae, and the sister group relationship of *Llanocetus* and Chaeomysticeti resulted from the analysis of Marx et al. (2015) on *Fucaia buelli*.

A noticeable difference is observed in the work by Fordyce & Marx (2018) who found that a clade formed by *Llanocetus* and *Mystacodon* represents the most basal mysticete clade with a more advanced position of Mammalodontidae in the tree. In this work, the monophyly of Mammalodontidae and Aetiocetide is not supported and the exclusion of *Morawanocetus* from Aetiocetidae questions the monophyly of this group.

Cisneros et al. (2018) maintained the monophyly of Mammalodontidae and Aetiocetidae but, in that work, this clade is the most basal mysticete clade and found that *Llanocetus* was the sister group of the stem Chaeomysticete taxa *Sitsqwayk* and *Tlaxcallicetus*.

Muizon et al. (2019) found another different solution in which *Mystacodon* is the most basal mysticete that is the sister group of a sequence of taxa formed by, respectively, *Coronodon*, *Llanocetus* and Aetiocetidae, being the last the sister group of Chaeomysticeti. Tsai & Fordyce (2018) found a monophyletic clade including *Coronodon*, Mammalodontidae and Aetiocetidae that was basal in their phylogeny of the mysticetes. They supported a sister group relationships between *Llanocetus* and Chaeomysticeti with *Toipahautea* nested well within basal chaeomysticetes. This solution represented a significant change from a previous paper published by Tsai & Fordyce

(2016) in which two different topologies were proposed depending on the search strategy of the most parsimonious tree: (a) a search based on unordered and unweighted characters resulted in *Llanocetus* being the most basal mysticete and the clade formed by Mammalodontidae and Aetiocetidae was the sister group of Chaeomysticeti, (b) a search based on weighted characters resulted in a clade formed by Mammalodontidae, Aetiocetidae and *Coronodon* as being the most basal mysticete group and in *Llanocetus* being the sister group of Chaeomysticeti.

This review shows that there are different opinions about the early evolution of mysticetes among students. Particularly debated are the relationships of *Llanocetus*, Aetiocetidae and Mammalodontidae and their relationships with Chaeomysticeti. Our results highlight the possibility that a single clade of early-diverging, toothed mysticetes diversified after its divergence from the ancestor it shared with Aetiocetidae, acknowledge the basal position of Mammalodontidae (according to, e.g., Bisconti & Carnevale, 2022) and suggests that Aetiocetidae was a primitive, well-diversified taxon that did not share a direct common ancestor with Chaeomysticeti.

4.2. Mysticete chronology in context

Most of the past attempts to infer divergence estimates for the main mysticete clades relied on some kind of molecular clock or total evidence analyses (Árnason et al., 2018; Marx and Fordyce, 2015; Geisler et al., 2011; McGowen et al., 2009; Steeman et al., 2009; Sasaki et al., 2005). This is the first attempt to provide divergence dates that are inferred based on occurrence data from fossiliferous localities all over the world. Our results are partially consistent with those provided by earlier studies as shown in Fig. S4 (Supplementary File 1). In particular, we observe that the dates proposed by previous studies for mysticete divergence range from *c.* 39 to *c.* 28 Ma and our hypothesis falls within the lower part of this range (*c.* 38 Ma). We believe that an older divergence date for mysticetes is in better agreement with the stratigraphic ages of earliest, toothed-mysticetes such as *Llanocetus* and *Mystacodon*; these species date back to about 33 Ma, thereby excluding younger divergence dates for mysticetes (such as *c.* 28 Ma as proposed by McGowen et al., 2009).

The age of divergence of the Chaeomysticeti ranges between *c.* 36 and *c.* 31 Ma with our result placed in around the middle part of this interval (*c.* 34 Ma; Fig. S4). All of these proposed dates suggest that the origin of baleen-assisted feeding in mysticetes evolved fast after the origin of the group. Based on our morphological dataset, a limited number of morphological transformations occurred at the transition to the Chaeomysticeti (Fig. 9; see also Bisconti and Carnevale, 2022), thus supporting the hypothesis that a limited amount of time is expected to be necessary to complete the structuring of the specialized character states diagnostic for the Chaeomysticeti.

The proposed estimated dates for the divergence of Balaenomorpha range from *c.* 35 and *c.* 23 Ma; our analysis resulted in a divergence date at *c.* 23 Ma (close to the Oligocene-Miocene boundary) (Fig. S4). Actually, there are no known balaenomorph mysticetes in the fossil record before the earliest Miocene. Even though this should be due to collection bias, the only two known taxa close to the Balaenomorpha (i.e., *Sitsqwayk cornishorum* and *Horopeta umarere*) show plesiomorphic character states supporting their exclusion from the Balaenomorpha. We interpret both *Sitsqwayk* and *Horopeta* as stem-Balaenomorpha. These two taxa are the only ones breaking the long branch that links the common ancestor of Balaenomorpha to the non-balaenomorph mysticetes, revealing that our knowledge of the evolution of stem-balaenomorph mysticetes is not fully adequate. Marx et al. (2019) observed this phenomenon and called it a ‘dark age’ of mysticete evolution but limited the stratigraphic extension of this interval to a few million years before and after the Oligocene-Miocene boundary and linked it to the faunal turnover that occurred when archaic mysticetes (including toothed mysticetes and earliest chaeomysticetes) went extinct and being replaced by balaenomorph mysticetes. We extend the cryptic period characterized by the absence of knowledge about the origin of Balaenomorpha to a time interval of *c.* 13 million years from *c.* 33 to *c.* 20 Ma. In this interval, the toothed mysticetes and early chaeomysticetes went extinct and the set of synapomorphies diagnostic of Balaenomorpha was assembled. We will discuss about biotic and abiotic forcing of this event later.

Based on literature, there is an interval of *c.* 16 million years between the older and the younger proposed divergence date of the crown Balaenidae. McGowen et al. (2009) provided a range included between 9.6 and 2.6 Ma that is at odd with fossil evidence suggesting that crown balaenids were already broadly present in European, North American and Japanese localities in the latest Miocene, thereby excluding the younger part of the proposed time interval. Sasaki et al. (2005) proposed an age of 17.1±3.5 Ma; the older part of this range is in good agreement with the presence of an early balaenoid from the early Miocene of Argentina (*Morenocetus parvus*; Buono et al., 2017). Our proposed divergence date places the origin of crown Balaenidae *c.* 7.3 Ma, which is in agreement with both our interpretation of *Morenocetus* as more closely related to *Caperea* than to Balaenidae and the balaenid fossil record (Bisconti et al., 2021a; Churchill et al., 2011). Previous hypotheses placed the divergence date of Balaenopteroidea in a range comprised between *c.* 18 and *c.* 11 Ma. Our result is more consistent with most of the balaenopterid fossil record and suggests that the balaenopteroids originated around 14 Ma. The taxonomic status and stratigraphic age of the early Miocene *Protororquaus dyticus*, a possible balaenopterid from the early Miocene of Argentina (see Bisconti and Bosselaers, 2021; Cabrera, 1926), is critical in this respect, as it could push back the origin of Balaenopteroidea by several million years, supporting an early Miocene origin of this group as suggested by Steeman et al. (2009).

4.3. Main mysticete evolutionary events and their relation to global dynamics

4.3.1. Origin and early evolution. Our results suggest that the origin of mysticetes occurred *c.*38 Ma. We were able to detect only a few factors fully concomitant with this event: (1) the opening of the Drake Passage, (2) explosive increase of *Chaetoceros* spores in the sedimentary record, and (3) increased Basin and Range volcanism (Figs 13, 14). The increased abundance of *Chaetoceros* spores suggests increased availability of food resources for pelagic fishes and macrozooplankton able to sustain populations of early, toothed-mysticetes. The opening of the Drake Strait between today Cape Horn and the South Shetland Islands and Antarctica was proposed long ago as a

possible trigger for the origin of mysticetes because this event activated the Circum-Antarctic Current that provides massive nutrient input to the planktonic communities of the Southern Hemisphere (Fordyce, 1977, 1980). At the time, this interpretation was based on the occurrence of the earliest mysticete fossils in New Zealand. It is not to be excluded that the nutrient injection by the volcanic activity and the early onset of the Circum-Antarctic Current acted as co-promoting factors in the setting of oceanic trophic chains with a remarkable increase of food availability. In this environmental context, the evolution of a novel predatory bauplan among cetaceans, that characteristic of early mysticetes, allowed the exploitation of newly developed trophic resources apparently without strong selective regimes. However, our work shows that the origin of the earliest mysticetes resulted from a period with high rate of morphological change (Fig. 9) that may be the result of directional selection. It is difficult to determine which of these two factors promoted the fast process leading to the assembly of the mysticete body plan (Bisconti and Carnevale 2022) even though the environmental context outlined above suggests that selection should have played a minor role in this process. Directional selection would result from loss of resources triggering strong competition but this does not seem the case for the origin of mysticetes, which occurred at a time of increased food resources.

Based on our results, the origin of chaeomysticetes (α_2 event) occurred around 28 Ma. The main factor that can be correlated with this event is a large phosphogenetic event (Fig. 14). Additional events are shown in Fig. 13 that could correlate with the α_1 event; these include the final phases of the opening of the Drake Passage, the opening of the Tasmania-Antarctica Passage and a number of volcanic events. The recent discovery of aetiocetid mysticetes in the North Pacific and of eomysticetid baleen whales in North and South Pacific, North Atlantic and Tethys suggests that one or more global factors promoted the origin and early diffusion of chaeomysticetes in these oceanic basins (Bisconti 2010). It cannot be excluded that the massive deposition of phosphorites occurring in the early Oligocene was related to the massive blooms of fish and plankton populations at worldwide scale. Large availability of food resources may have set a comfortable environmental

context in which even a low rate of morphological change (Fig. 9) promoted the assembly of the chaeomysticete body plan characterized by the presence of elongated rostra, baleen for filter-feeding, loss of radial crest from the radius and change in orientation of the olecranon process of the ulna (Bisconti and Carnevale 2022); these characters affect the methods used by mysticetes to access food resources through direct catch and swimming behaviors.

Interestingly, there is no apparent competition dynamics in the curve depicting the 'evolutionary faunas' around 34 Ma but, rather, earliest chaeomysticetes and toothed mysticetes coexisted without apparent interference. This observation suggests that there was no niche overlap and, therefore, the earliest baleen-bearing mysticetes exploited different trophic sources from those exploited by toothed mysticetes. An accurate analysis of the feeding biomechanics of toothed- and baleen-bearing mysticetes would be highly desirable to test this hypothesis. Tsai and Kohno (2016) and Tsai and Ando (2016) suggested that a process of niche partitioning took place during the time interval of existence of the Aetiocetidae as they were able to show that there was an observable interval of size variation in this group at the end of the Oligocene.

The origin of chaeomysticetes should be regarded as an evolutionary process leading a group to invade a new trophic niche by means of novel morphological and functional characteristics. This process occurred through low rate of morphological change within an environmental context rich in food resources as testified by massive global deposition of phosphorites, increased diatom diversity and high values of $\delta^{13}C$ with respect to the previous few million years and, most notably, with apparent lack of competition between toothed- and early baleen-bearing mysticete species.

4.3.2. Miocene diversification events. Analysis of clade diversity suggests that the origin of crown-mysticetes (Balaenomorpha) occurred at the very end of the Chattian (latest Oligocene), at a time when toothed- and early baleen-bearing mysticetes underwent a worldwide, massive extinction process without a corresponding replacement events (Figs 5, 6). This cryptic 'dark age' of mysticete evolution was also documented by Marx et al. (2019) who suggested that differential survival of

mysticete species depended on the habitat they inhabited with oceanic species being more likely to survive than more coastal species. Marx et al. (2019) observed also a drop in diversity in some odontocete groups, with the extinction of certain groups such as the Xenorophiidae, and suggested that the sea level rise, between the latest Oligocene and the end of the Aquitanian (Fig. 9), was responsible for the loss of the coastal niches necessary to sustain whales living more inshore. Both origination and extinction rates were null in this period thus suggesting that a sampling bias could affect our knowledge of mysticete diversity. Further exploration of latest Oligocene-to-Early Miocene fossiliferous horizons at global scale will confirm or dismantle this hypothesis but, currently, we must assume that only a limited number of mysticetes survived the extinctions at the end of the Oligocene and gave rise to Balaenomorpha.

The analysis of the rates of morphological change showed that only a few transformations occurred between the common ancestor of Chaeomysticeti and *Horopeta umarere*, one of the earliest stem-balaenomorph mysticetes, but a high number of morphological changes occurred from the common ancestor of *Horopeta* + Balaenomorpha and the common ancestor of Balaenomorpha. This suggests that the early steps leading to the novel architectures of stem-balaenomorph mysticetes were relatively few but a high number of transformation events (Fig. 9) were necessary for the complete assembly of the balaenomorph body plan. These changes occurred in less than 4.5 Ma suggesting the existence of a directional selection active during the earliest Oligocene-to-Early Miocene. Apparently, there was not a competitive dynamics underlying this phase as the documented diversity of balaenomorph mysticetes (as documented by both fossil record and clade diversity) remained low until the end of the Aquitanian, *c.* 20 Ma (Fig. 9). By that epoch, balaenomorph mysticetes underwent an explosive radiation through the fast divergence of Balaenoidea and Thalassotherii, two clades characterized by profoundly different trophic strategies and biomechanics.

The β event, corresponding to the origin and early differentiation of Balaenomorpha, occurred after a period of temperature instability during which stem-balaenomorph mysticetes began to appear in

the oceans. A peak in origination rate is recorded around 20 Ma based on clade diversity, suggesting that most of the early diversification of Balaenomorpha occurred without increased extinction rate (Fig. 6). For the first time, it is possible to observe an increase in body size (Fig. 10) suggesting that the differentiation between alternative filter feeding mechanisms was paralleled by a niche partitioning process that generated a wider body size range among mysticetes. The end of one of the main phosphogenetic episodes of the Cenozoic occurred just about 20 Ma (Fig. 14) at a time when the major clades of Balaenomorpha were just established. We found that a peak in $\delta^{13}C$ is recorded at about 23 Ma that is followed by a slight drop in $\delta^{13}C$ suggesting a decrease of the primary production in the oceans during the Aquitanian. Based on these observations, we found that two indicators indicate reduced oceanic productivity in the earliest Miocene suggesting that sharp selective regimes were active by the end of the Chattian and the end of the Aquitanian. At the end of this period, the fossil record shows that a process of niche partitioning was completed among baleen-bearing mysticetes with the establishment of continuous ram feeding Balaenoidea and intermittent ram feeding stem Thalassotherii (Fig. 4). Interestingly, several speciation events occurred within some of the most representative krill genera, *Euphausia* (Jarman et al. 2000) and *Nyctiphanes* (D'Amato et al. 2008) between 26 and 16 Ma. The possible diversification of euphausiids in the late Aquitanian and Burdigalian (Fig. 14) is concomitant with the origin of intermittent ram feeding mysticetes belonging to basal thalassotherian taxa (Kimura 2002) suggesting the existence of a possible causal link between these two events. However, there are no data about the feeding strategies of the predicted stem thalassotherian taxa (not still found in the fossil record but supposed to have existed by phylogenetic analysis) suggesting that it is not possible to test this tempting hypothesis at the moment.

We observe a consistent diversification of thalassotherian taxa starting from *c.* 20 Ma (Fig. 5), approximately at the same time when a massive diversification of oceanic lantern fishes took place. We dissected this mysticete radiation by realizing curves depicting 'evolutionary faunas' (Fig. 8) and observe that the overall radiation is constituted by different processes affecting the diversity of

the different balaenomorph families. We observe two pulses of diversity increase of basal thalassotherian taxa at *c.* 20 and *c.* 16 Ma. Then, the diversity of basal thalassotherians decreases and that of Cetotheriidae increases suggesting a strong competitive regime between these two families. Currently, the feeding behavior of Cetotheriidae is under debate with two different hypotheses being supported by different sources of evidence: (a) piscivory supported by the find of an isolated fish aggregate among the ribs of a Miocene cetotheriid mysticete in Peru (Collareta et al. 2015) and (b) bottom feeding supported by reconstruction of muscular attachments on the dentary and skull of *Herpetocetus morrowi* (El Adli et al. 2014). Based on the data plotted in Fig. 8 we are more inclined to suppose that piscivory was shared by both basal thalassotherians and cetotheriids but, even in this case, a more complete understanding of the feeding biomechanics of these mysticetes is required to test the hypothesis of competition that we propose to explain the shape of the curve of the 'evolutionary faunas' showing contemporaneous decline in basal thalassotherians and rise of cetotheriid mysticetes.

Starting from about 14 Ma, we observe an initial decline of the Cetotheriidae contemporaneous to an initial rise of balaenopterid mysticetes (δ event of Fig. 4; Fig. 8). Even in this case, the curve suggests that a strong competitive regime was acting and balaenopterids resulted more well equipped to survive this regime. The initial increase of Balaenopteridae is synchronous with an increase in diatom diversity and with geodynamic events (Fig. 13) suggesting an increased complexity of the oceanic ecosystems. We suspect that there is a causal link between the peak of balaenopterid diversity observed between 8 and 9 Ma and the almost contemporaneous peaks in dissolved Si and detrital input (Fig. 12), suggesting that more nutrients were available for plankton and, therefore, more food (notably planktic diatoms) was available in the oceanic trophic webs. The apparent competitive exclusion of Cetotheriidae from access to trophic resources operated by balaenopterids is probably related to the increased efficiency of food removal performed by the latter thanks to specialized biomechanical features of the feeding apparatus in the skull and mandible (Sanderson and Wassersug 1993).

4.3.3. Pliocene-to-Recent events.

Even though the Pliocene was characterized by relatively high diversity in mysticetes (mostly due to the increased numbers of balaenid and balaenopterid species), the end of the Pliocene experienced an impoverishment of the mysticete faunas all around the world (Fig. 5). Geodynamic and climatic events approximately synchronous with this pattern include a major temperature drop (starting from *c.* 2.5 Ma) and large-scale oscillations in sea level that may have impacted on the availability of coastal areas for reproduction and feeding of small-sized species (Figs 12, 14). In this time interval, we observe a massive increase in mean body size with the origin and stabilization of gigantic species (*sensu* Bisconti et al. 2021). Earlier occurrences of large-sized and gigantic mysticetes are here regarded as occasional results of isolated phylogenetic lineages.

As a matter of fact, in the last 5 million years we observe the extinction of Cetotheriidae, a pulse in balaenid diversity followed by a drop, and a pulse in balaenopterid diversity followed by a drop after 2.5 Ma. Eschrichtiids (the gray whale) and neobalaenids (the pygmy right whale) maintained a reduced diversity throughout the period. Apparently, the only factors concomitant with the observed pattern are the drop in temperature, eustatic oscillations and the closure of the Central America Seaway with the consequent onset of the Gulf Stream that started to transfer warm waters to the Northern Hemisphere in different way with respect to the late Miocene. These factors were already evidenced by Whitmore (1994) and we support his conclusions with our results. We add the observation that the temperature drop was not only associated to a body size increase but, rather, to a trend toward an expansion in body size range that is still represented among living mysticetes. Based on our phylogenetic results, for instance, the origin of the minke whale (*Balaenoptera acutorostrata*) corresponds to a miniaturization process from large-sized ancestors (Fig. 11), showing that during the Plio-Pleistocene there was not a single trend in body size change. Actually, in the late Pliocene and Pleistocene we observe the widest range of body sizes in the whole evolutionary history of mysticetes and this suggests the establishment of a considerable niche

partitioning between the species still inhabiting the oceans as body size has long been considered a straightforward proxy for ecology and niche partitioning (Tsai and Ando, 2016; Damuth and MacFadden, 1990). This inference is supported by the different alimentary specializations of the balaenopterid species of the northern hemisphere that feed upon specific prey items (different fish and krill species; Kawamura 1980), a pattern that is still showing evolutionary trends in the oceans of today (Gavrilchuk et al. 2014; Ryan et al. 2013).

Conclusions

The evolutionary history of baleen whales is punctuated by several diversification events. We provided a new chronological framework where these events can be included in order to understand when major origination and extinction pulses occurred and when mysticete body size changed significantly. We used a newly-generated phylogenetic analysis to infer ancestral sizes at internal nodes in order to obtain good chronological assessments of all the events. The inference of chronology depended on (a) an extensive review of the locality of discovery of fossil mysticetes based on a dataset that included more than 1400 entries and (b) a statistical method based on sampling intensity of taxa in the localities discussed above. The main chronological results include: (1) the origin of the mysticetes: *c.* 38 Ma; (2) the origin of the Chaeomysticeti: *c.* 34 Ma; (3) origin of Balaenomorpha: *c.* 24 Ma; (4) origin of Balaenoidea (pygmy, right and bowhead whales): *c.* 23.3 Ma; (5) origin of Thalassotherii: *c.* 19.9 Ma; (6) origin of Balaenopteroidea (rorquals, humpbacks and gray whales): *c.* 13.9 Ma.

Major origination pulses occurred about 38 Ma, between Bartonian and Priabonian in the Eocene; about 28 Ma, between Rupelian and Chattian in the Oligocene; and several times since the Aquitanian. Major extinction pulses occurred between the Rupelian and the Aquitanian (extinction of toothed mysticetes and earliest chaeomysticetes, including Eomysticetidae), and during the interval comprised between the Tortonian and the Pliocene. The analysis of ‘evolutionary faunas’ revealed distinct competition regimes between basal thalassotherians and Cetotheriidae and between

Cetotheriidae and Balaenopteridae, suggesting that Cetotheriidae, basal thalassotherians and Balaenopteridae occupied similar trophic niches. Apparently, no competition dynamics is observed in the Eocene and Oligocene between toothed mysticetes and early chaeomysticetes (mainly formed by the Eomysticetidae), supporting the hypothesis that these groups fed in different ways.

Rates of morphological changes varied throughout mysticete evolution. Higher rates are observed at the transition from Archaeocetes to Mysticetes, at the origin of Balaenomorpha, at the origin of Thalassotherii, at the origin of Cetotheriidae and at the origin of Balaenopteroidea. Body size diversity begins to expand from the Tortonian but the highest rates of body size change occurred in the Pleistocene, leading to the origin of gigantic mysticetes still living today.

There is not a single mechanism explaining all the evolutionary events discussed in this paper. We found that different events show relationships with different biotic or abiotic events such as geodynamic events (e.g., onset of circum-Antarctic current, wide and strong volcanism, etc.) and biological events (e.g., increase in diatom diversity and abundance).

We provided a wealth of new data and interpretations in terms of chronology and analysis of the main drivers in mysticete evolution (extinction/origination rates, rates of size change, morphological, taxonomic and clade diversity, major diversification events etc.) and provided a global framework to chronologically and biologically interpret the evolution of baleen whales.

Acknowledgments

This work was supported by grants (ex-60% 2021 and 2022) from the Università degli Studi di Torino. Many thanks are due to Mark D. Uhen who provided suggestions about statistical literature in an early stage of this research. Mark D. Uhen and Toshiyuki Kimura provided accurate reviews of this paper greatly improving its scientific content and clarity; we want to warmly thank them for their effort. Last but not least, we want to thank Alessandra Negri for her constructive and efficient editorial support.

References

Aït-Hamou, F., Dautria, J.M., Cantagrel, J.M., Dostal, J., Briqueu, L., 2000. Nouvelles données géochronologiques et isotopiques sur le volcanisme cénozoïque de l'Ahaggar (Sahara algérien): des arguments en faveur d'un panache. Comptes Rendus Académie Sciences Paris 330 (12), 829-836. https://doi.org/10.1016/S1251-8050(00)00217-2

Alroy, J., 2014. Accurate and precise estimates of origination and extinction rates. Paleobiology 40, 374–397.

Árnason, U., Lammers, F., Kumar, V., Nilsson, M.A., Janke A., 2018. Whole-genome sequencing of the blue whale and other rorquals finds signatures for introgressive gene flow. Sci. Adv. 4, eaap987.

Bajpai, S., Gingerich, P.D., 1998. A new Eocene archaeocete (Mammalia, Cetacea) from India and the time of origin of whales. PNAS 95, 15464–15468.

Bannister, J.L., 2009. Baleen whales. In: Perrin, W.F., Würsig, B., Thewissen, J.G.M. (Eds.), Encyclopedia of Marine Mammals. Academic Press, San Diego, Pp. 62–72.

Barron, J.A., 2022. Refined assessment of the paleoceanographic and tectonic influences on the deposition of the Monterey Formation in California. In: Aiello, I., Barron, J.A., Ravelo, C. (eds.), Understanding the Monterey Formation and similar biosiliceous units across space and time. Geological Society of America Special Papers. https://doi.org/10.1130/2022.2556(06)

Barros, N.B., Clarke, M.R., 2002. Diet. In: Perrin, W.F., Würsig, B., Thewissen, J.G.M. (Eds.), Encyclopedia of Marine Mammals. Academic Press, San Diego, pp. 323–327.

Berge, J., Gabrielsen, T.M., Moline, M., Renaud, P.E., 2012**.** Evolution of the Arctic *Calanus* complex: an Arctic marine avocado? J. Plankton Res. 34, 191–195.

Berta, A., Lanzetti, A., 2020. Feeding in marine mammals: An integration of evolution and ecology through time. Palaeontol. Electronica 23, a40.

Betka, P.M., Thomson, S.N., Sincavage, R., Zoramthara, C., Lalremruatfela, C., Lang, K.A., Steckler, M.S., Bezbaruah, D., Borgohain, P., Seeber, L., 2021. Provenance shift during

Neogene Brahmaputra Delta progradation tied to coupled climate and tectonic change in the Eastern Himalaya. Geochemistry, Geophysics, Geosystems 22, e2021GC010026. https://doi.org/10.1029/2021GC010026

Bianucci, G., Marx, F.G., Collareta, A., Di Stefano, A., Landini, W., Morigi, C., Varola, A., 2019 Rise of the titans: baleen whales became giants earlier than thought. Biol. Lett. 15, 20190175.

Bisconti, M., 2007. A new basal balaenopterid from the Early Pliocene of northern Italy. Palaeontology 50, 1103–1122.

Bisconti, M., 2010. Cenozoic environmental changes and evolution of baleen whales. In: Murray, C.A. (Ed.), Whales and dolphins. Behavior, biology and distribution. Nova Publishers, New York, pp. 1–46.

Bisconti, M., Bosselaers, M.E.J., 2020. A new balaenopterid species from the Southern North Sea Basin informs about phylogeny and taxonomy of *Burtinopsis* and *Protororqualus* (Cetacea, Mysticeti, Balaenopteridae). PeerJ 8, e9570.

Bisconti, M., Carnevale, G., 2022. Skeletal Transformations and the Origin of BaleenWhales (Mammalia, Cetacea,Mysticeti): A Study on Evolutionary Patterns. Diversity, 14, 221. https://doi.org/10.3390/d14030221

Bisconti, M., Munsterman, D.K., Post, K., 2019. A new balaenopterid whale from the late Miocene of the Southern North Sea Basin and the evolution of balaenopterid diversity (Cetacea, Mysticeti). PeerJ 7, e6915.

Bisconti, M., Pellegrino, L., Carnevale, G., 2021. Evolution of gigantism in right and bowhead whales (Cetacea: Mysticeti: Balaenidae). Biol. J. Linn. Soc. 134, 498–524.

Bisconti, M., Raineri, G., Tartarelli, G., Monegatti, P., Carnevale, G., 2022. The periotic of a basal balaenopterid from the Tortonian of the Stirone River, northern Italy (Cetacea, Mysticeti, Balaenopteridae). Palaeobiodiv. Palaeoenv. https://doi.org/10.1007/s12549-022-00550-2

Boessenecker, R.W., 2013. A new marine vertebrate assemblage from the Late Neogene Purisima Formation in Central California, part II: pinnipeds and cetaceans. Geodiversitas 35, 815–940.

Boone, S.C., Balestrieri, M.L., Kohn, B., 2021. Tectono-thermal evolution of the Red Sea Rift. Frontiers in Earth Science (9), 713448. https://doi.org/10.3389/feart.2021.713448

Boscolo-Galazzo, F., Jones, A., Dunkley Jones, T., Crichton, K.A., Wade, B.S., Pearson, P.N., 2022. Late Neogene evolution of modern deep-dwelling plankton. Biogeosciences 19, 743-762. https://doi.org/10.5194/bg-19-743-2022

Bromham, L., 2019. Six impossible things before breakfast: assumptions, models and belief in molecular dating. Trends in Ecol. Evol. 34, 474–484.

Brusatte, S.L., Montanari, S., Yi, H.-y, Norell, M.A., 2011. Phylogenetic corrections for morphological disparity analysis: new methodology and case studies. Paleobiology 37, 1-22.

Buono, M.R., Fernandez, M.S., Cozzuol, M.A., Cuitiño, J.I., Fitzgerald, E.M.G., 2017. The early Miocene balaenid *Morenocetus parvus* from Patagonia (Argentina) and the evolution of right whales. PeerJ 5, e4148.

Cabrera, A., 1926. Cetaceos fosiles del Museo de La Plata. Rev. Mus. la Plata 29, 363–411.

Cather, S.M., Chapin, C.E., Kelley, S.A., 2012. Diachronous episodes of Cenozoic erosion in southwestern North America and their relationship to surface uplift, paleoclimate, paleodrainage, and paleoaltimetry. Geosphere 8 (6), 1177-1206. https://doi.org/10.1130/GES00801.1

Cermeño, P., Falkowski, P.G., Romero, O.E., Schaller, M.F., Vallina, S.M., 2015. Continental erosion and the Cenozoic rise of marine diatoms. Proceedings National Academy of Sciences U.S.A. 112 (14), 1–6. https://doi.org/10.1073/pnas.1412883112

Churchill, M., Berta, A., Deméré, T., 2012. The systematic of right whales (Mysticeti: Balaenidae). Mar. Mam. Sci. 28, 497–521.

Collareta, A., Landini, W., Lambert, O., Post, K., Tinelli, C., Di Celma, C., Panetta, D., Tripodi, M., Salvadori, P.A., Caramella, D., Marchi, D., Urbina, M., Bianucci, G., 2015. Piscivory in a Miocene Cetotheriidae of Peru: first record of fossilized stomach content for an extinct baleen-bearing whale. Sci. Nat. 102, 70.

Cortese, G., Gersonde, R., Hillenbrand, C.D., Kuhn, G., 2004a. Opal sedimentation shifts in and progression of the Messinian salinity crisis. Nature 400, 652–655. http://doi.org/10.1038/23231

Cortese, G., Gersonde, R., Hillenbrand, C.-D., Kuhn, G. 2004b. the World Ocean over the last 15 Ma. Earth Planet. Sci. Lett. 224, 509–527. http://doi.org/10.1016/10.1016/j.epsl.2004.05.035

Couvreur, T.L.P., Dauby, G., Blach-Overgaard, A., Deblauwe, V., Dessein, S., Droissart, V., Hardy, O.J., Harris, D.J., Janssens, S.B., Ley, A.C., Mackinder, B.A., Sonké, B., Sosef, M.S.M., Stévart, T., Svenning, J.C., Wieringa, J.J., Faye, A., Missoup, A.D., Tolley, K.A., Nicolas, V., Ntie, S., Fluteaeu, F., Robin, C., Guillocheau, F., Barboni, D., Sepulchre, P., 2020. Tectonics, climate and the diversification of the tropical African terrestrial flora and fauna. Biological Reviews 96 (1), 16-51. https://doi.org/10.1111/brv.12644

D'Amato, M.E., Harkins, G.W., de Oliveira, T., Teske, P.R., Gibbons, M. J., 2008. Molecular dating and biogeography of the neritic krill *Nyctiphanes*. Mar. Biol. 155, 243-247.

Damuth, J.D., MacFadden, B.J., 1990. Body Size in Mammalian Paleobiology: Estimation and Biological Implications. Cambridge University Press, Cambridge

Deméré, T.A., McGowen, M.R., Berta, A., Gatesy, J.. 2008. Morphological and molecular evidence for a stepwise evolutionary transition from teeth to baleen in mysticete whales. Syst. Biol. 57, 15–37.

Dickinson, J.A., Wallace, M.W., Holdgate, G.R., Gallagher, S.J., Thomas, L., 2002. Origin and timing of the Miocene-Pliocene unconformity in Southeast Australia. Journal of Sedimentary Research 72 (2), 288-303.

Dominici, S., Danise, S., Cau, S., Freschi, A., 2020. The awkward distribution of fossil whales. Earth-Science Reviews 205, 103057.

Døssing, A., Japsen, P., Watts, A.B., Nielsen, T., Jokat, W., Thybo, H., Dahl-Jensen, T., 2016. Miocene uplift of the NE Greenland margin linked to plate tectonics: seismic evidence from the Greenland Fracture Zone, NE Atlantic. Tectonics 35, 257-282. https://doi.org/10.1002/2015TC004079

Droser, M.L., 2003. Ecological changes through geological time. In: Briggs, D.E.G., Crowther, P.R. (Eds), Palaeobiology II. Blackwell Publishing, Malden, pp. 432–437

Ekdale, E.G., Deméré, T.A., 2021. Neurovascular evidence for a co-occurrence of teeth and baleen in an Oligocene mysticete and the transition to filter-feeding in baleen whales. Zool. J. Linn. Soc. 194, 395–415.

El Adli, J.J., Deméré, T.A., Boessenecker, R.W., 2014. *Herpetocetus morrowi* (Cetacea: Mysticeti), a new species of diminutive baleen whale from the Upper Pliocene (Piacenzian) of California, USA, with observations on the evolution and relationships of the Cetotheriidae. Zool. J. Linn. Soc. 170, 400–466.

Elshaafi, A., Gudmundsoon, A., 2021. Central volcanoes and caldera collapses in the late Miocene-Late Pleistocene Tibesti Volcanic Province, northwest Chad. Journal of Geodynamics 145, 101846. https://doi.org/10.1016/j.jog.2021.101846

Figueiredo, J., Hoorn, C., van der Ven, P., Soares, E., 2009. Late Miocene onset of the Amazon River and the Amazon deep-sea fan: evidence from the Foz do Amazonas Basin. Geology 37, 619-622. https://doi.org/10.1130/G25567A.1

Filippelli, G.M., 1997. Intensification of the Asian monsoon and a chemical weathering event in the late Miocene-early Pliocene: implications for the late Neogene climate change. Geology 25 (1), 27-30. http://doi.org/10.1130/0091-7613(1997)025<0027:IOTAMA>2.3.CO;2

Fordyce, R.E., 1980. Whale evolution and Oligocene Southern Ocean environments. Palaeogeogr. Palaeoecol. Palaeocl. 31, 319–336.

Fordyce, R.E., 1977. The development of the circum-Antarctic current and the evolution of the Mysticeti (Mammalia: Cetacea). Palaeogeogr. Palaeoecol. Palaeocl. 21,265–271.

Fordyce, R.E., Marx, F.G., 2018. Gigantism precedes filter feeding in baleen whale evolution. Curr. Biol. 28, 1670–1676.

Galloway, W.E., Witheaker, T.L., Ganey-Curry, P., 2011. History of Cenozoic North American drainage basin evolution, sediment yield, and accumulation in the Gulf of Mexico basin. Geology 7 (4), 938-973. https://doi.org/10.1130/GES00647.1

Gatesy, J., Ekdale, E.G., Deméré, T.A., Lanzetti, A., Randall, J., Berta, A., El Adli, J., Springer, M.S., McGowen, M.R., 2022. Anatomical, ontogenetic, and genomic homologies guide reconstructions of the teeth-to-baleen transition in mysticete whales. BioRxiv preprint doi: https://doi.org/10.1101/2022.03.10.483660

Gavrilchuk, K., Lesage, V., Ramp, C., Sears, R., Bérubé, M., Bearhop, S., Beauplet, G., 2014. Trophic niche partitioning among sympatric baleen whale species following the collapse of groundfish stocks in the Northwest Atlantic. Mari. Ecol. Progr. Ser. 497, 285–301.

Geisler, J.H., McGowen, M.R., Yang, G., Gatesy, J., 2011. A supermatrix analysis of genomic, morphological, and paleontological data from crown Cetacea. BMC Evol. Biol. 11, 1–33.

Gingerich, P.D., Uhen, M.D., 1998. Likelihood estimation of the time of origin of Cetacea and the time of divergence of Cetacea and Artiodactyla. Palaeontol. Electronica https://doi.org/10.26879/98008

Gladstone, R., Flecker, R., Valdes, P., Lunt, D., Marwick, P., 2007. The Mediterranean hydrologic budget from a Late Miocene global climate simulation. Palaeogeography, Palaeoclimatology, Palaeoecology 251, 254–267. http://doi.org/10.1016/j.palaeo.2007.03.050

Goldbogen, J.A., Cade, D.E., Wisniewska, D.M., Potvin, J., Segre, P.S., Savoca, M.S., Hazen, E.L., Czapanskiy, M.F., Kahane-Rapport, S.R., Deruiter, S.L., Gero, S., Tønnesen, P., Gough, W.T., Hanson, M.B., Holt, M.M., Jensen, F.H., Simon, M., Stimpert, A.K., Arranz, P., Johnston, D.W., Nowacek, D.P., Parks, S.E., Visser, F., Friedlaender, A.S., Tyack, P.L., Madsen, P.T., Pyenson, N.D., 2019. Why whales are big but not bigger: physiological drivers and ecological limits in the age of ocean giants. Science 366, 1367–1372.

Goloboff, P.A., Catalano, S.A., 2016. TNT version 1. 5, including a full implementation of phylogenetic morphometrics. Cladistics 32, 231–238.

Griffin, D.L., 2002. Aridity and humidity: two aspects of the late Miocene climate of North Africa and the Mediterranean. Palaeogeography, Palaeoclimatology, Palaeoecology 182, 65–91.

Griffin, D.L., 2006. The late Neogene Sahabi rivers of the Sahara and their climatic and environmental implications for the Chad Basin. Journal of the Geological Society 163, 905–921.

Guo, Z.T., Ruddiman, W.F., Hao, Q.Z., Wu, H.B., Qiao, Y.S., Zhu, R.X., Peng, S.Z., Wei, J.J., Yuan, B.Y., Liu, T.S., 2002. Onset of Asian desertification by 22 Myr inferred from loess deposits in China. Nature 416, 159-163. https://doi.org/10.1038/416159a

Hammer, Ø., Harper, D.A.T., Ryan, P.D., 2001. PAST: paleontological statistics software package for education and data analysis. Palaeontol. Electronica 4, 4.

Haq, B.U., Hardenbol, J., Vail, P.R., 1987. Chronology of fluctuating sea levels since the Triassic. Science 235, 1156–1167. https://doi.org/10.1126/science.235.4793.1156

http://doi.org/10.1016/S0031-0182(01)00453-9

Hocking, D.P., Marx, F.G., Park, T., Fitzgerald, E.M.G., Evans, A.R., 2017. A behavioural framework for the evolution of feeding in predatory aquatic mammals. Proc. R. Soc. B 284, 20162750. http://dx.doi.org/10.1098/rspb.2016.2750

Huelsenbeck, J.P., 1994. Comparing the stratigraphic record to estimates of phylogeny. Paleobiology 20, 470–483.

Hyeong, K., Kim, J., Yoo, C.M., Moon, J.W., Seo, I., 2013. Cenozoic history of phosphogenesis recorded in the ferromanganese crusts of central and western Pacific seamounts: implications for deepwater circulation and phosphorus budgets. Palaeogeography, Palaeoclimatology, Palaeoecology 392, 293-301. https://doi.org/10.1016/j.palaeo.2013.09.012

Jarman, S.N., Elliott, N.G., Nicol, S., McMinn, A., 2000. Molecular phylogenetics of circumglobal *Euphausia* species (Euphausiacea: Crustacea). Can. J. Fish. Aq. Sci. 57 (Suppl. 3). 51–58.

Jordan, T.E., Kirk-Lawlor, N.E., Blanco, N., Rech, J.A., Cosentino, N.J., 2014. Landscape modification in response to repeated onset of hyperarid paleoclimate states since 14 Ma,

Atacama Desert, Chile. Geological Society of America Bulletin 126 (7-8), 1016-1046. https://doi.org/10.1130/B30978.1

Katz, O., 2019. Conflict and complementarity of paleontological and molecular chronologies? Paleobiology 45, 7–20.

Kawamura, A., 1980. A review of food of balaenopterid whales. Sci. Rep. Whales Res. Inst. 32, 155–197.

Keller, G., Barron, J.A., 1983. Paleoceanographic implications of Miocene deep-sea hiatuses. Geological Society of America Bulletin 94, 590-613.

Kemp, A.E.S., Pearce, R.B., Grigorov, I., Rance, J., Lange, C.B., Quilty, P., Salter, I., 2006. Production of giant marine diatoms and their export at oceanic frontal zones: implications for Si and C flux from stratified oceans. Global Biogeochemical Cycles 20 (4), 1-13. https://doi.org/10.1029/2006GB002698

Kimura, T., 2002. Feeding strategy of an early Miocene cetothere from the Toyama and Akeyo Formations, central Japan. Palaeontol. Res. 6, 179–189.

Kooistra, W.H.C.F., Gersonde, R., Medlin, L.K., Mann, D.G., 2007. The origin and evolution of the diatoms: their adaptation to a planktonic existence. In: Evolution of Primary Producers in the Sea (P.G. Falkowski, A.H. Knoll), Academic Press, pp. 207-249.

Kouwenhoven, T.J., van der Zwaan, G.J., 2006. A reconstruction of late Miocene Mediterranean circulation patterns using benthic foraminifera. Palaeogeography, Palaeoclimatology, Palaeoecology 238 (1), 373–385. http://doi.org/10.1016/j.palaeo.2006.03.035

Krijgsman, W., Hilgen, F.J., Raffi, I., Sierro, F.J., Wilson, D.S., 1999a. Chronology, causes

Maddison, W., Maddison, D., 2019. Mesquite 3.61: a modular system for evolutionary analysis. Available at: https://www.mesquiteproject.org/

Marx, F.G., Buono, M.R., Evans, A.R., Fordyce, R.E., Reguero, M., Hocking, D.P., 2019a. Gigantic mysticete predators roamed the Eocene Southern Oceans. Antarct. Sci. 31, 98–104.

Marx, F.G., Fordyce, R.E., 2015. Baleen boom and bust: a synthesis of mysticete phylogeny, diversity and disparity. Roy. Soc. Open Sci. 2, 140434.

Marx, F.G., Fitzgerald, E.M.G., Fordyce, R.E., 2019b. Like phoenix from the ashes: how modern baleen whales arose from a fossil "dark age". Acta Palaeontol. Pol. 64, 231–238.

Marx, F.D., Hocking, D., Park, T., Ziegler, T., Evans, A.R., Fitzgerald, E.M.G., 2016. Suction feeding preceded filtering in baleen whale evolution. Memoirs of Museum Victoria 75:71-81.

Marx, F.G., Uhen, M.D., 2010. Climate, critters, and cetaceans: Cenozoic drivers of the evolution of modern whales. Science 327, 993–996.

Matzke, N.J., Irmis, R.B., 2016. Including autapomorphies is important for paleontological tip-dating with clocklike data, but not with non-clock data. PeerJ 6:e4553; DOI 10.7717/peerj.4553

McGowen, M.R., Spaulding, M., Gatesy, J., 2009. Divergence date estimation and a comprehensive molecular tree of extant cetaceans. Mol. Phyl. Evol. 53, 891–506.

Mouthereaeu, F., 2011. Timing of uplift in the Zagros belt/Iranian plateau and accommodation of late Cenozoic Arabia-Eurasia convergence. Geological Magazine 148 (5-6), 726-738. https://doi.org/10.1017/S0016756811000306

Muizon, C. de, Bianucci, G., Martínez-Cáceres, M., Lambert, O., 2019. *Mystacodon selenensis*, the earliest known toothed mysticete (Cetacea, Mammalia) from the late Eocene of Peru: anatomy, phylogeny, and feeding adaptations. Geodiversitas 41, 401–499.

Ollier, C.D., Pain, C.F., 2019. Neotectonic mountain uplift and geomorphology. Geomorfologiya 4, 3-26. https://doi.org/10.31857/S0435-4281201943-26

O'Leary, M., Uhen, M.D., 1999. The time of origin of whales and the role of behavioral changes in the terrestrial-aquatic transition. Paleobiology 25, 534–556.

Pellegrino, L., Dela Pierre, F., Natalicchio, M., Carnevale, G., 2018. The Messinian diatomite deposition in the Mediterranean and its relationships to the global silica cycle. Earth-Science Reviews 178, 154-176. https://doi.org/10.1016/j.earscirev.2018.01.018

Peredo, C.M., Pyenson, N.D., Boersma, A.T., 2017. Decoupling tooth loss from the evolution of baleen in whales. Front. Mar. Sci. 4, 67. doi: 10.3389/fmars.2017.00067

Peredo, C.M., Pyenson, N.D., Uhen, M.D., 2022. Lateral palatal foramina do not indicate baleen in fossil whales. Sci. Rep., 11448.

Pérez-Escobar, O.A., Zizka, A., Bermúdez, M.A., Meseguer, A.S., Condamine, F.L., Hoorn, C., Hooghiemstra, H., Pu, Y., Bogarín, D., Boschman, L.M., Pennington, R.T., Antonelli, A., Chomicki, G., 2022. The Andes through time: evolution and distribution of Andean floras. Trends in Plant Science 27 (4), 364-378. https://doi.org/10.1016/j.tplants.2021.09.010

Pershing, A.J., Christensen, L.B., Record, N.R., Sherwood, G.D., Stetson, P.B., 2010. The impact of whaling on the ocean carbon cycle: why bigger was better. PLoS ONE 5, e12444.

Pershing, A.J., Stamieszkin, K., 2020. The North Atlantic ecosystem, from plankton to whales. Annu. Rev. Mar. Sci. 12, 339–359.

Potter, P.E., Szatmari, P., 2009. Global Miocene tectonics and the modern world. Earth-Science Reviews 96, 279-295. https://doi.org/10.1016/j.earscirev.2009.07.003

Potter, P.E., Szatmari, P., 2015. The global Middle and Late Miocene and the deep earth: model for earlier orogenies. Marine and Petroleum Geology 68, 178–191. https://doi.org/10.1016/j.marpetgeo.2015.08.021

Pyenson, N.D., Sponberg, S.N., 2011. Reconstructing body size in extinct crown cetacea (Neoceti) using allometry, phylogenetic methods and tests from the fossil record. J. Mam. Evol. 18, 269–289.

Rea, D.K., 1992. Delivery of Himalayan sediment to the northern Indian Ocean and its relation to global climate sea level, uplift, and seawater strontium. In: Duncan, R.A., Rea, D.K., Kidd, R.B., von Rad, U., Weissel, J.K., (Eds.), Synthesis of Results from Scientific Drilling in the Indian Ocean. Geophysical Monograph 70, American Geophysical Union, 387-402.

Renaudie, J., 2016. Quantifying the Cenozoic marine diatom deposition history: links to the C and Si cycles. Biogeosciences 13, 6003-6014. https://doi.org/10.5194/bg-13-6003-2016

Rivadeneira, M., Hunt, G., Roy K., 2009. The use of sighting records to infer species extinctions: an evaluation of different methods. Ecol. 90, 1291–1300.

Rognon, P., Gourinard, Y., Bandet, Y., Koeniguer, J.C., Delteil-Desneux F., 1983. Précisions chronologiques sur l'évolution volcano-tectonique et géomorphologiques de l'Atakor (Hoggar): apports des données radiométriques (K/Ar) et paléobotaniques (bois fossiles). Bulletin Société Géologique France 25, 973-980.

Rohling, E.J., Marino, G., Grant, K.M., 2015. Mediterranean climate and oceanography, and the periodic development of anoxic events (sapropels). Earth-Science Reviews 143, 62-97. https://doi.org/10.1016/j.earscirev.2015.01.008

Roman, J,. Palumbi, S.R., 2003. Whales before whaling in the North Atlantic. Science 301, 508–510.

Rooney, A., Honeycutt, R.L., Derr, J.N., 2001. Historical population size change of bowhead whales inferred from DNA sequence polymorphism data. Evolution 55, 1678–1685.

Ryan, C., McHugh, B., Trueman, C.N., Sabin, R. et al., 2013 Stable isotope analysis of baleen reveals resource partitioning among sympatric rorquals and population structure in fin whales. Mar. Ecol. Prog. Ser. 479, 251–261.

Sanderson, L.R., Wassersug, R., 1993. Convergent and alternative designs for vertebrate suspension feeding. In: Hanken, J., Hall, B.K. (Eds.), The skull: functional and evolutionary mechanisms (volume 3). University Press of Chicago, Chicago, pp. 37–112.

Santini, F., Carnevale, G., 2015. First multilocus and densely sampled timetree of trevallies, pompanos and allies (Carangoidei, Percomorpha) suggests a Cretaceous origin and Eocene radiation of a major clade of piscivores. Molecular Phylogenetics and Evolution 83, 33-39.

Santini, F., Carnevale, G., Sorenson, L., 2013. First molecular scombrid timetree (Scombridae, Percomorpha) shows recent radiation of tunas following invasion of pelagic habitats. Italian Journal of Zoology 80, 210-221.

Sarkar, S., Basak, C., Frank, M., Berndt, C., Huuse, M., Badhani, S., Bialas, J., 2019. Late Eocene onset of the Proto-Antarctic Circumpolar Current. Scientific Reports 9 (10125), 1-10. https://doi.org/10.1038/s41598-019-46253-1

Sasaki, T., Nikaido, M., Hamilton, H., Goto, M., Kato, H., Kanda, N., Pastene, L.A., Cao, Y., Fordyce, R.E., Hasegawa, M., Okada, N., 2005. Mitochondrial phylogenetics and evolution of mysticete whales. Syst. Biol. 54, 77–90.

Savoca, M.S., Czapanskiy, M.F., Kahane-Rapport, S.R., Gough, W.T., Fahlbusch, J.A., Bierlich, K.C., Segre, P.S., Di Clemente, J., Penry, G.S., Wiley, D.N., Calambokidis, J., Nowacek, D.P., Johnston, D.W., Pyenson, N.D., Friedlaender, A.S., Hazen, E.L., Goldbogen, J.A., 2021. Baleen whale prey consumption based on high-resolution foraging measurements. Nature 599, 85–90.

Schuster, M., Duringer, P., Ghienne, J.F., Vignaud, P., Mackaye, H.T., Likius, A., Brunet, M., 2006. The age of the Sahara Desert. Science 311, 821. https://doi.org/10.1126/science.1120161

Schwarzhans, W., Carnevale, G., 2021. The rise to dominance of lanternfishes (Teleostei: Myctophidae) in the oceanic ecosystems: a paleontological perspective. Paleobiology 47 (3), 446-463. https://doi.org/10.1017/pab.2021.2

Scotese, C.R., Song, H., Mills, B.J.W., van der Meer, D.G., 2021. Phanerozoic paleotemperatures: the Earth's changing climate during the last 540 million years. Earth-Science Reviews 215, 103503. https://doi.org/10.1016/j.earscirev.2021.103503

Senut, B., Pickford, M., Ségalen, L., 2009. Neogene desertification of Africa. Comptes Rendus Geoscience 341, 591-602. https://doi.org/10.1016/j.crte.2009.03.008

Sepkoski, J.J. Jr, 1981. A factor analytic description of the Phanerozoic marine fossil record. Paleobiology 7, 36–53.

Sepulchre, P., Ramstein, G., Fluteaeu, F., Schuster, M., Tiercelin, J.J., Brunet, M.J., 2006. Tectonic uplift and Eastern Africa aridification. Science 313 (5792), 1419-1423. http://doi.org/10.1126/science.1129158

Slater, G.J., Goldbogen, J.A., Pyenson, N.D., 2017. Independent evolution of baleen whale gigantism linked to Plio-Pleistocene ocean dynamics. Proc. Roy. Soc. B 284, 20170546.

Smith, T.J., Puttick, M.N., O'Reilly, J.E., Pisani, D., Donoghue, P.C.J., 2021. Phylogenetic sampling affects evolutionary patterns of morphological disparity. Palaeontology 64, 765-787.

Soltis, P.S., Soltis, D.E., 2003. Applying the bootstrap in phylogeny reconstruction. Stat. Sci. 18, 256-267.

Steeman, M.E., Hebsgaard, M.B., Fordyce, R.E., Ho, S.Y.W., Rabosky, D.L., Nielsen, R., Rahbek, C., Glenner, H., Sørensen, M., Willerslev, E., 2009. Radiation of extant cetaceans driven by restructuring of the oceans. Syst. Biol. 58,573–585.

Steinthorsdottir, M., Coxall, H.K., de Boer, A.M., Huber, M., Barbolini, N., Bradshaw, C.D., Burls, N.J., Feakins, S.J., Gasson, E., Henderiks, J., Holbourn, A.E., Kiel, S., Kohn, M.J., Knorr, G., Kürschner, W.M., Lear, C.H., Liebrand, D., Lunt, D.J., Mörs, T., Pearson, P.N., Pound, M.J., Stoll, H., Strömberg, C.A.E., 2021. The Miocene: the Future of the Past. Paleoceanography and Paleoclimatology 36, e2020PA004037. https://doi.org/10.1029/2020PA004037

Sternai, P., Caricchi, L., Pasquero, C., Garzanti, E., van Hinsbergen, D.J.J., Castelltort, S., 2019. Magmatic forcing of Cenozoic climate? Journal of Geophysical Research: Solid Earth 125, e2018JB016460. https://doi.org/10.1029/2018JB016460

Strauss, D., Sadler, P.M. 1989. Classical confidence intervals and Bayesian probability estimates for ends of local taxon ranges. Math. Geol. 21, 411–427.

Strömberg, C.A.E., Staver, A.C., 2022. The history and challenge of grassy biomes. Science 377 (6606), 592-593. https://doi.org/10.1126/science.add1347

Suto, I., 2006. The explosive diversification of the diatom genus Chaetoceros across the Eocene/Oligocene and Oligocene/Miocene boundaries in the Norwegian Sea. Marine Micropaleontology 58, 259-269. https://doi.org/10.1016/j.marmicro.2005.11.004

Tsai, C.-H., Ando, T., 2016. Niche partitioning in Oligocene toothed mysticetes (Mysticeti: Aetiocetidae). J. Mam. Evol. 23, 33–41.

Tsai, C.-H., Kohno, N., 2016. Multiple origins of gigantism in stem baleen whales. Sci. Nat. 103, 89 10.1007/s00114-016-1417-5

Vidal, V., Bonneville, A., 2004. Variations of the Hawaiian hot spot activity revealed by variations in the magma production rate. Journal of Geophysical Research 109, B03104. https://doi.org/10.1029/2003JB002559

Wang, S.C., Marshall, C.R., 2016. Etimating times of extinction in the fossil record. Biol. Lett. 122015098920150989. http://doi.org/10.1098/rsbl.2015.0989

Whitmore, F.C. Jr., 1994. Neogene climatic change and the emergence of the modern whale fauna of the North Atlantic Ocean. In: Berta, A., Deméré, T.A. (Eds.), Contributions in marine mammal paleontology honoring Frank C. Whitmore, Jr. Proc. San Diego Soc. Nat. Hist. 29: 233–227.

Willett, S.D., 2010. Late Neogene erosion of the Alps: a climate driver? The Annual Review of Earth and Planetary Sciences 38, 411-437. https://doi.org/10.1146/annurev-earth-040809-152543

Witkowski, J., Bryłka, K., Bohaty, S.M., Midłowska, E., Penman, D.E., Wade, B.S., 2021. North Atlantic marine biogenic silica accumulation through the early-to-mid Paleogene: implications for ocean circulation and silicate weathering feedback. Climate of the Past, 1-25. https://doi.org/10.5194/cp-2021-50

Zachos, J., Pagani, M., Sloan, L., Thomas, E., Billups, K., 2001. Trends, rhythms, and aberrations in global climate 65 Ma to Present. Science 292 (5517), 686-693. https://doi.org/10.1126/science.1059412

Zheng, H., 2016. Asia dust production ramped up since latest Oligocene driven by Tibetan Plateau uplift. National Science Review 3 (3), 271-274.

Captions to illustrations

Figure 1. Stratigraphic distributions of mysticete species based on data downloaded from the Paleobiology Database. Main mysticete groups are indicated. The thick lines correspond to FAD and LAD for species represented by more than one specimen, and, for species represented by the holotype only, to the errors of the estimations of the geological age of such a specimen. Scale generated through TSCreator visualization of enhanced Geologic Time Scale 2016 database (Version 7.4; 2022), James Ogg (database coordinator) https://engineering.purdue.edu/Stratigraphy/tscreator.

Figure 2. Strict consensus (Nelsen) cladogram resulting from the present paper with indication of bootstrap (bold numbers) and symmetric resampling (regular numbers) supporting values, and main mysticete clades.

Figure 3. Phylogenetic relationships of mysticete family-rank clades obtained by collapsing internal nodes of monophyletic groups shown in Figure 2. Main mysticete suprafamily clades are indicated.

Figure 4. Phylogenetic relationships of family- and suprafamily-rank mysticete clades plotted against a temporal scale showing the stratigraphic distributions of the groups and main diversification events in yellow ellipses. In this plot, the thick lines are drawn based on all the available data including FAD and LAD of species represented by more than one specimen, and the error in the estimation of the geological age of the holotype in species represented by only one specimen.

Figure 5. Plots illustrating the changes in diversity occurred throughout mysticete evolutionary history against a temporal scale. A, alpha diversity based on fossil and extant species occurrences. B, clade diversity. The main diversification events are indicated by Greek letters.

Figure 6. Patterns of extinction and origination throughout the mysticete evolution. **a**, alpha origination rates per million years. **b**, clade origination rates per million years. **c**, alpha extinction rates per million years. **d**, clade extinction rates per million year.

Figure 7. Phylogenetic relationships of mysticetes plotted against a temporal scale with indication of main mysticete clade. Phylogenetic relationships are from cladogram in Figure 3 and analysis from present paper. Thin lines represent ghost lineages. Thick lines represent all the available intormation about the stratigraphic distributions of the species: FAD and LAD for species represented by more than one specimen, and error in the estimation of the geological ages of the holotypes for species represented by one specimen only. Note that the times of origin of main clades (at internal nodes) are those reported in Table 1.

Figure 8. 'Evolutionray faunas'. Plots comparing occurrences and clade numbers of different mysticete family-rank clades against a temporal scale showing diversity trends and eventual competition dynamics. Greek and Latin letters between the two plots represent major diversification events presented in Figure 4.

Figure 9. Rates of morphological changes at particular transition events throughout mysticete evolution.

Figure 10. Box plot showing body size change throughout mysticete evolution. White circles correspond to outliers.

Figure 11. Ancestral state reconstruction and evolution of body size in mysticetes. Blue corresponds to small size (total length < 8 m); yellow corresponds to middle size (total length included between 9 and 13 m); orange corresponds to large size (total length included between 14

and 20 m); red corresponds to gigantic size (total length > 20 m). Thick lines represent stratigraphic distributions of species generated by taking in mind all the available information including FAD and LAD for species represented by more than one specimen, and error in the estimation of the geological ages of the holotypes for species represented by one specimen only.

Figure 12. Mysticete body size and clade diversity compared to: CO_2 concentration – Renaudie (2016); global average temperature (LOWI: Late Oligocene Warm Interval; EMCI: Early Miocene Cool Interval; MMTM: Middle Miocene Thermal Maximum; LMCI: Late Miocene Cool Interval; MG: Messinian Glaciations; PTM: Pliocene Thermal Maximum; LGM: Last Glacial Maximum; PIA: Pleistocene Ice Age) – Scotese et al. (2021); ice-sheet evolution – Zachos et al. (2001); sea level – Haq et al. (1987); carbon isotopes – Zachos et al. (2001); diatom abundance and diversity – Renaudie (2016); strontium isotopes – Renaudie (2016); sediment yield – Sternai et al. (2021); detrital contribution vs. eolian quartz – Zheng (2016); dissolved silicon flux – Cermeño et al. (2015).

Figure 13. Mysticete body size and clade diversity compared to: terrestrial ecosystems evolution comprising grasslands (1: first open-habitat grass in North America; 2: first grass-dominated habitat in North America; 3: first grass-dominated habitat in Africa; 4: first open-habitat grass in Australia; 5: first grass-dominated habitat in Australia) – Strömberg & Staver (2022), grazers (1: first common in North America; 2: first common in Africa; 3: first common in Australia) – Strömberg & Staver (2022), fires (1: increase in Australia; 2: increase in Africa) – Strömberg & Staver (2022) and deserts (1: onset of Asian desertification – Guo et al., 2002; 2: onset of Namib desert – Senut et al., 2009; 3: onset of Atacama desert – Jordan et al., 2014; 4: onset of Sahara desert – Schuster et al., 2006); global rates of ridge spreading – Potter and Szatmari (2009); main tectonic and volcanic events occurred in Africa (Red Sea rifting – Boone et al., 2021; Hoggar volcanism – Rognon et al., 1983; Aït-Hamou et al., 2000; Tibesti volcanic province – Elshaafi & Gudmundsson, 2021; onset of

modern Congo river drainage, Ethiopian traps, Southern African Escarpment, uplift of Central African Atlantic Swell, East African Rift System – Couvreur et al., 2020; acceleration of East African Plateau – Sepulchre et al., 2006); Americas (Basin and Range volcanism – Sternai et al., 2021; Columbia River flood basalt – Steinthorsdottir et al., 2021; Yellowstone Hotspots – Potter & Szatmari, 2015; Southwestern N. America uplift – Cather et al., 2012; Great Basin Ignimbrites – Sternai et al., 2021; Southern Cordillera uplift – Cather et al., 2012; Andean orogeny, acceleration of Andean uplift – Pérez-Escobar et al., 2022; Drake Passage opening, Panama Isthmus shoaling – Potter and Szatmari, 2015; Amazon Fan sedimentation rate – Figueiredo et al., 2009; Gulf of Mexico clastic deposition – Galloway et al., 2011; Eurasia (Bengal and Nicobar Fan sedimentation rate – Betka et al., 2021; Tethys closure – Potter & Szatmari, 2015; enhanced erosion of Alps – Willett, 2010; Greenland-Scotland Ridge opening – Potter & Szatmari, 2015; Himalayan orogeny - Cermeño et al., 2015; Tibetan-Plateau uplift increase, Greenland-Scotland Ridge opening – Potter & Szatmari, 2015; further acceleration of Himalaya uplift – Filippelli, 1997; N. Indian Ocean sediment influx – Rea, 1992; Mediterranean-Atlantic gateways closure – Kouwenhoven & van der Zwaan, 2006; strong increase of riverine runoff in the Mediterranean – Griffin, 2002, 2006, Gladstone et al., 2007; increase of circum-Mediterranean volcanism, Burma Basin, Mekong River, Red River, South China Margin, East China Margin clastic deposition – Potter and Szatmari, 2015; Hawaiian magma flux – Vidal & Bonneville, 2004; Zagros uplift increase – Mouthereau, 2011; Iceland Plume volume flux – Døssing et al., 2016; Oceania (Development of New Zealand Alpine Fault, Tasmania-Antarctic Passage opening, Indonesian gateways closure - Potter & Szatmari, 2009, 2015; tectonic activity in SE Australian basins, uplift of Papua New Guinea – Dickinson et al., 2002).

Figure 14. Mysticete body size and ‘evolutionary faunas’ compared to oceanographic events and ecological turnovers in marine environment comprising: major phosphogenetic episodes – Hyeong et al. (2013); radiation of deep dwelling planktic foraminifera (Boscolo-Galazzo et al., 2022);

increase of high productivity-adapted benthic foraminifera (Steinthorsdottir et al., 2021); low-to-mid latitude diatom decline, Indian Ocean diatom increase – Renaudie (2016); full establishment of Southern Ocean opal belt – Renaudie (2016); Oligocene-Miocene Carbon Maximum – Steinthorsdottir et al. (2021); Atlantic to Pacific silica switch (uncertainties about the onset are indicated by question marks) – Keller & Barron, (1983), Barron (2022); Late Miocene Carbon Isotope Shift, Monterey Event – Steinthorsdottir et al. (2021); opal deposition in S. Pacific – Sarkar (2019); Monterey event – Steinthorsdottir et al. (2021); Messinian Salinity Crisis – Krijgsman et al. (1999); explosive *Chaetoceros* resting spore diversification and abundance in N. Atlantic, further *Chaetoceros* spore diversification in N. Atlantic and *Chaetoceros* spore drop in N. Atlantic – Suto (2006); Carbonate Crash, Late Miocene-Early Pliocene Biogenic Bloom – Steinthorsdottir et al. (2021); 1st significant opal deposition in Southern Ocean – Renaudie (2016); giant diatom ooze deposition in the oceans – Kemp et al. (2006); onset of coastal mid-latitude upwelling – Renaudie (2016); cyclical sapropelitic deposition in the Mediterranean – Rohling et al. (2015); NCW/NADW, AACC – Sarkar et al. (2019), Steinthorsdottir et al. (2021); Euphasiaceae evolution (1: divergence of *Nyctiphanes* clade; 2: common ancestor of *Nyctiphanes* species; 3: most recent common ancestor of *Nyctiphanes australis*, *N. capensis* and *N. couchii*; 4: most recent common ancestor of *N. australis* and *N. capensis*) – D'Amato et al. (2008); Diaphinae evolution – Schwarzhans & Carnevale (2021).